

An improved calculation of the $D_{(s)}^* D_{(s)} V$ and $B_{(s)}^* B_{(s)} V$ couplings from light-cone sum rules

Su-Ping Jin ^{*a} and Hua-Yu Jiang ^{†a}

^aSchool of Physics, Nankai University, Weijin Road 94, 300071 Tianjin, China

March 21, 2024

Abstract

We present an improved calculation of the $D_{(s)}^* D_{(s)} V$ and $B_{(s)}^* B_{(s)} V$ coupling constants, where V denotes ρ , K^* , ω , and ϕ meson. These couplings govern the QCD long-distance dynamics in interactions between heavy pseudoscalar/vector mesons and light vector mesons. Our analysis is conducted within the framework of QCD light-cone sum rules (LCSRs) by utilizing the light-cone distribution amplitudes (LCDAs) of light vector mesons. By systematically incorporating the subleading power corrections and higher-twist contributions at leading order (LO) and including the next-to-leading order (NLO) corrections at leading power, we achieve enhanced accuracy in the light-cone operator product expansion (OPE) for the underlying correlation function. In assessing the reliability of the established LCSRs, we consider uncertainties arising from the choice of the quark-hadron duality region in the double dispersion relation. Building upon these improvements, we accomplish an optimized computation and analysis for the strong coupling constants g_{H^*HV} which are used to extract the effective coupling λ in the heavy meson chiral perturbation theory (HM χ PT). Furthermore, we investigate the $SU(3)$ flavour symmetry breaking effects in detail and compare our sum rule calculations with previous studies in an exploratory way.

*jinsuping@nankai.edu.cn

†huayujiang@nankai.edu.cn

Contents

1	Introduction	3
2	Light-cone Sum Rules for the $D_{(s)}^*D_{(s)}V$ and $B_{(s)}^*B_{(s)}V$ couplings	5
3	Double spectral density of the correlation function	8
3.1	Double spectral density at LO	8
3.2	Double spectral density at NLO	12
4	Quark-hadron duality and sum rules	15
5	Numerical analysis	18
6	Conclusion	32
7	Acknowledgments	34
A	The definitions of the vector meson LCDAs	34
B	Parameterizations for the vector meson DAs	36
C	Double spectral density and integral at NLO	40
	References	41

1 Introduction

The strong couplings among the heavy vector mesons ($D_{(s)}^*$ or $B_{(s)}^*$ meson), the heavy pseudoscalar mesons ($D_{(s)}$ or $B_{(s)}$) and the light vector mesons (V involving ρ , K^* , ω and ϕ), represented by g_{D^*DV} and g_{B^*BV} , offer valuable insights into the non-perturbative aspects of the long-distance dynamics within quantum chromodynamics (QCD). By combining the chiral and heavy quark symmetry of QCD, the heavy meson chiral perturbative theory (HM χ PT) [1–4] provides an effective framework to describe interactions between heavy and light mesons at low energy. The $D_{(s)}^*D_{(s)}V$ and $B_{(s)}^*B_{(s)}V$ couplings are essential ingredients for the extraction of the effective coupling parameter λ which governing the H^*HV interactions in the HM χ PT Lagrangian [3, 5].

Furthermore, the $D_{(s)}^*D_{(s)}V$ and $B_{(s)}^*B_{(s)}V$ couplings play a crucial role in determining the residue of the vector and tensor form factors for $D \rightarrow V$ and $B \rightarrow V$ transitions at the D^* and B^* poles, as dictated by the dispersion relation [6–9]. This insight enhances our understandings of the behavior of these form factors, which are vital for extracting the CKM parameters and the lepton flavour universality (LFU) parameters in the $D \rightarrow V\ell\nu$ and $B \rightarrow V\ell\nu$ semileptonic decays. Moreover, the $D_{(s)}^*D_{(s)}V$ couplings are crucial for understanding the final-state interactions (FSIs), which can make significant contributions to the long-distance dynamics and may contribute strong phases, potentially leading to direct CP violation in B meson non-leptonic decays [5].

Due to the phase space limit, direct experimental measurements of these couplings are not feasible. Consequently, some couplings, particularly $g_{B^*B\rho}$ and g_{D^*DV} , have been determined through calculations employing QCD techniques such as SVZ sum rules (QCDSRs) [10–12] and light-cone sum rules (LCSRs) [13–15]. However, these calculations, mainly conducted at leading order [16–23], often come with relatively large uncertainties. Recently, significant progress has been made in calculating the correlation functions using QCD (SCET) factorization approach in light-cone sum rules [24]. Incorporating next-to-leading order (NLO) (α_s) corrections and subleading power (Λ/m_Q) contributions has granted us the ability to more precisely determine the spectral density of the dispersion relation for building up the LCSRs. This approach has been widely used to calculate some essential non-perturbative physical quantities, for instance, the heavy-to-light ($B \rightarrow \pi$, etc.) and heavy-to-heavy ($B \rightarrow D$, etc.) transition form factors. The calculation of the correlation function based on QCD (SCET) factorization is carried out from two-distinct aspects: the hard-collinear factorization by using the light-cone distribution amplitudes (LCDAs) of light hadrons, such as in [25–29], and a slightly more complex factorization procedure by separating the hard, hard-collinear, collinear and soft scales with the using of the heavy-light hadrons LCDAs, e.g., the calculations in [30–38].

The QCD (SCET) factorization-based LCSRs has emerged as a robust technique for investigating strong couplings beyond leading order and power like $g_{H^*H\rho}$ [8], and $g_{H^*H\pi}$ [9]. The higher-

order/power contributions can significantly affect the magnitude of strong couplings, potentially altering the overall results by approximately 10% to 20% for NLO and 20% to 30% for subleading-power effects as shown in [8]. However, discrepancies between calculation results in LCSRs [8, 16–18] and the extrapolated coupling $g_{B^*B\rho}$ from $B \rightarrow \rho$ form factors [28, 32], using dispersion relation, have been observed. These discrepancies may stem from incomplete analyses of subleading power contributions at leading order (LO) and next-to-leading order (NLO) contributions at higher-twist, along with uncertainties arising from different shapes of the duality region at NLO [9]. Another potential explanation for this inconsistency is the inclusion of contributions from excited heavy meson states to the dispersion relation [39], which introduces considerable model dependence and raises questions about effectively isolating ground-state contributions within the duality region.

Given the importance of these strong couplings for our understanding of QCD long-distance dynamics, as introduced previously, this paper aims to present a comprehensive investigation of the $D_{(s)}^*D_{(s)}V$ and $B_{(s)}^*B_{(s)}V$ strong couplings using LCSRs. The essential new ingredients are summarized as follows.

- We improve the calculation accuracy of the established light-cone sum rules from two perspectives. Firstly, we incorporate more complete subleading power corrections¹ (up to δ_V^4 , δ_s^1 , and $(\delta_V\delta_s)^1$) and higher-twist corrections (up to two-particle twist-5 and three-particle twist-4) of the LCDAs of light vector mesons at leading order and the NLO contributions at leading-power. Secondly, we consider the uncertainties due to the choice of the quark-hadron duality region in the double dispersion relation, an aspect which was not addressed in the previous study [8]. Based on these enhancements, we present the optimized and comprehensive computations for the $D_{(s)}^*D_{(s)}V$ and $B_{(s)}^*B_{(s)}V$ couplings to date. This enables us to obtain a more accurate prediction for the effective coupling λ of the HM χ PT, which still exhibits significant deviation from the estimation provided by the vector meson dominance (VMD) model [40].
- We conduct a detailed investigation into the impact of $SU(3)$ flavour ($SU(3)_F$) symmetry breaking effects, which stem from modifications in the light quark mass, the decay constants and mass of the vector mesons and heavy mesons, and the parameters related to the vector meson LCDAs. Our analysis indicates that the $SU(3)_F$ breaking effects play a non-negligible role in accurately determining the coupling constants $g_{H_s^*HK^*}$, $g_{H^*H_sK^*}$, $g_{H^*H\omega}$ and $g_{H_s^*H_s\phi}$. As expected, the most significant breaking effects are observed in the coupling $g_{H_s^*H_s\phi}$, primarily due to the involvement of the maximum number of strange quarks in this channel.

¹We define $\delta_V \equiv m_V/m_Q$, $Q = (b, c)$ and $\delta_s \equiv m_s/m_V$ (m_V denotes the mass of vector mesons, m_Q and m_s are respectively the heavy and strange quark mass). A detailed discussion on the effectiveness of our power expansion is presented in Table 5.

- We investigate the dispersion relation, which establishes a connection between the residue of various $B_{(s)} \rightarrow V$ transition form factors (for V and T_1) at the $B_{(s)}^*$ pole and the corresponding $B_{(s)}^* B_{(s)} V$ strong coupling. The couplings $g_{B_{(s)}^* B_{(s)} V}$, accompanied by systematic uncertainties, are computed from the dispersion relation using form factors obtained from two distinct LCSR methods [28, 32].

We update all input parameters utilized in LCSRs. Specifically, we employ the RunDec package [41] to adopt the four-loop evolution values for the QCD coupling and quark mass within the $\overline{\text{MS}}$ scheme. The decay constants of vector and pseudoscalar heavy-light mesons are determined using two distinct methods: QCD two-point sum rules [9, 42] with the same NLO accuracy as the LCSRs, and lattice QCD (LQCD) [43, 44].

The structure of this paper is organized as follows: In section 2, we introduce the conventions and definitions for the $D_{(s)}^* D_{(s)} V$ and $B_{(s)}^* B_{(s)} V$ couplings and establish the corresponding LCSRs using the double dispersion relation. In section 3, we present the calculation details for the LO and NLO double spectral density of the correlation function. Section 4 is dedicated to discussing the uncertainties arising from the quark-hadron duality ansatz for the double dispersion relation and constructing the finalized form of the LCSRs. We focus on determining the various input parameters and analyzing the numerical results in section 5. The final section concludes the work. Essential details regarding the vector meson LCDAs are provided in Appendices A and B, while Appendix C contains expressions for the double spectral densities at NLO.

2 Light-cone Sum Rules for the $D_{(s)}^* D_{(s)} V$ and $B_{(s)}^* B_{(s)} V$ couplings

Our study begins with the introduction of the phenomenological effective Lagrangian [3–5] governing the strong interactions between heavy mesons and light vector resonances,

$$\mathcal{L}_{eff} = -\frac{1}{2} g_{H^* H V} \epsilon_{\mu\nu\alpha\beta} (\partial^\mu V^\nu)^i_j \left(H_i^\dagger \overleftrightarrow{\partial}^\alpha H^{*\beta j} - H_i^{*\beta\dagger} \overleftrightarrow{\partial}^\alpha H^j \right), \quad (1)$$

with the convention $\epsilon_{0123} = -1$, $g_{H^* H V}$ represents the strong couplings, and V stands for the nonet matrix of vector mesons,

$$V = \begin{pmatrix} \frac{\rho^0}{\sqrt{2}} + \frac{\omega}{\sqrt{2}} & \rho^+ & K^{*+} \\ \rho^- & -\frac{\rho^0}{\sqrt{2}} + \frac{\omega}{\sqrt{2}} & K^{*0} \\ K^{*-} & \bar{K}^{*0} & \phi \end{pmatrix}, \quad (2)$$

and $H^{(*)} = (D^{(*)0}, D^{(*)+}, D_s^{(*)+})$ or $(B^{(*)-}, \bar{B}^{(*)0}, \bar{B}_s^{(*)0})$. The hadronic matrix element of the effective Lagrangian, describing the coupling between specific initial and final states, plays a crucial role

in determining the strength of the interaction between particles in a given process,

$$\langle V(p, \eta^*) H^*(p+q, \varepsilon) | \mathcal{L}_{eff} | H(q) \rangle = -g_{H^*HV} \epsilon_{\alpha\beta\rho\sigma} \eta^{*\alpha} \varepsilon^{*\beta} p^\rho q^\sigma, \quad (3)$$

where the vector meson $V(p, \eta)$ is characterized by its mass m_V , 4-momentum p , and polarization vector η . These couplings are determined by the charge and flavour quantum numbers of the initial and final hadrons. In this work, we focus on the couplings $g_{D^{*+}D^0\rho^+}$, $g_{D^{*+}D^+\omega}$, $g_{D_s^{*+}D^0K^{*+}}$, $g_{D_s^{*+}D_s^+\bar{K}^{*0}}$ and $g_{D_s^{*+}D_s^+\phi}$ in the charm sector, as well as $g_{\bar{B}^{*0}B^-\rho^+}$, $g_{B^{*0}D^0\omega}$, $g_{\bar{B}_s^{*0}B^-K^{*+}}$, $g_{\bar{B}^{*0}\bar{B}_s^0\bar{K}^{*0}}$ and $g_{\bar{B}_s^{*0}\bar{B}_s^0\phi}$ in the bottom sector. The others can be related to the aforementioned couplings through isospin symmetry, which dictates certain relationships between couplings involving particles with different isospin quantum numbers,

$$\begin{aligned} \text{D case : } \quad g_{D^*D\rho} &\equiv g_{D^{*+}D^0\rho^+} = -\sqrt{2}g_{D^{*+}D^+\rho^0} = \sqrt{2}g_{D^{*0}D^0\rho^0} = -g_{D^{*0}D^+\rho^-}, \\ g_{D_s^*DK^*} &\equiv g_{D_s^{*+}D^0K^{*+}} = -g_{D_s^{*+}D^+K^{*0}}, \quad g_{D^*D_sK^*} \equiv g_{D_s^{*+}D_s^+\bar{K}^{*0}} = g_{D^{*0}D_s^+K^{*-}}; \end{aligned} \quad (4)$$

$$\begin{aligned} \text{B case : } \quad g_{B^*B\rho} &\equiv g_{\bar{B}^{*0}B^-\rho^+} = -\sqrt{2}g_{\bar{B}^{*0}\bar{B}^0\rho^0} = \sqrt{2}g_{B^{*-}B^-\rho^0} = -g_{B^{*-}\bar{B}^0\rho^-}, \\ g_{B_s^*BK^*} &\equiv g_{\bar{B}_s^{*0}B^-K^{*+}} = -g_{\bar{B}_s^{*0}\bar{B}_s^0K^{*0}}, \quad g_{B^*B_sK^*} \equiv g_{\bar{B}^{*0}\bar{B}_s^0\bar{K}^{*0}} = g_{B_s^{*-}\bar{B}_s^0K^{*-}}. \end{aligned} \quad (5)$$

In the more general $SU(3)$ flavour symmetry framework, specific relations exist for the D and B cases. These relations govern certain patterns or constraints on the interactions between particles within the D and B meson sectors, based on their shared properties under $SU(3)$ transformations,

$$\text{D case : } \quad g_{D^*D\rho} = g_{D_s^*DK^*} = g_{D^*D_sK^*} = g_{D_s^*D_s\phi} = \sqrt{2}g_{D^*D\omega}; \quad (6)$$

$$\text{B case : } \quad g_{B^*B\rho} = g_{B_s^*BK^*} = g_{B^*B_sK^*} = g_{B_s^*B_s\phi} = \sqrt{2}g_{B^*B\omega}. \quad (7)$$

To establish the sum rules for the coupling g_{H^*HV} , we adopt the approach outlined in Ref.[37]. This involves investigating the correlation function between the vacuum and V -meson, utilizing two distinct local interpolating currents for vector and pseudoscalar heavy mesons, denoted by j_μ and j_5 . These currents are employed to effectively probe the relevant properties and dynamics of the heavy meson sector,

$$F_\mu(p, q) = i \int d^4x e^{-i(p+q)\cdot x} \langle V(p, \eta^*) | T\{j_\mu(x), j_5(0)\} | 0 \rangle = \epsilon_{\mu\nu\rho\sigma} \eta^\nu p^\rho q^\sigma F((p+q)^2, q^2). \quad (8)$$

Here, $j_\mu = \bar{q}_1 \gamma_\mu Q$ and $j_5 = (m_Q + m_{q_2})\bar{Q} i \gamma_5 q_2$, where the heavy quark, denoted as Q , corresponds to either c or b , while $q_{1,2}$ represent one of the light quarks, u , d , or s .

Following [45], one can utilize the analytic properties of the amplitude in two distinct invariant variables: $(p+q)^2$ and q^2 , corresponding to the squared momenta of interpolating currents in the

two channels. By incorporating the complete sets of intermediate states with quantum numbers of H and H^* into these channels, we derive the double dispersion relation,

$$F_\mu(p, q) = \frac{\langle V(p, \eta) H^*(p+q, \varepsilon) | H(q) \rangle \langle H(q) | j_5 | 0 \rangle \langle H^*(p+q, \varepsilon) | j_\mu | 0 \rangle}{[(p+q)^2 - m_{H^*}^2] [q^2 - m_H^2]} + \dots \quad (9)$$

It's worth noting that we have omitted the continuum part in this derivation.

To establish the LCSRs for the strong coupling constant, we begin by substituting its definition and expressing the matrix elements of interpolating currents in terms of the decay constants f_H and f_{H^*} . Subsequently, we derive the double dispersion relations for the amplitude $F((p+q)^2, q^2)$,

$$F((p+q)^2, q^2) = -\frac{g_{H^*HV} f_{H^*} f_H m_H^2 m_{H^*}}{[m_{H^*}^2 - (p+q)^2] [m_H^2 - q^2]} + \iint_{\Sigma} \frac{\rho_{cont}(s_1, s_2) ds_1 ds_2}{[s_1 - (p+q)^2] (s_2 - q^2)} + \dots \quad (10)$$

The relevant matrix elements used to define the heavy meson decay constants are outlined as follows:

$$\langle 0 | j_5 | H(p) \rangle = f_H m_H^2, \quad \langle H^*(p+q, \varepsilon) | j_\mu | 0 \rangle = f_{H^*} m_{H^*} \varepsilon_\mu. \quad (11)$$

The leading term in Eq. (10) represents the contribution from the ground-state double-pole, which involves the product of the desired strong coupling g_{H^*HV} and the corresponding decay constants. The term $\rho_{cont}(s_1, s_2)$ captures the combined spectral density of excited and continuum states, and Σ denotes the duality region occupied by these states in the (s_1, s_2) -plane. Additional terms resulting from subtractions, represented by ellipses, vanish after the application of the double Borel transformation.

In QCD, the invariant function $F((p+q)^2, q^2)$ can be calculated at momentum transfers q^2 and $(p+q)^2$ much smaller than the heavy quark mass m_Q^2 through the light-cone OPE applied to the correlation function (8) near the light-cone $x^2 \sim 0$. The result can be factorized in terms of the convolution of a hard kernel and the LCDAs of vector mesons, classified by their twist. The former represents the short-distance perturbative contributions, while the latter parameterizes the long-distance non-perturbative effects. The OPE calculations can be represented in the form of a double dispersion relation:

$$F^{(\text{OPE})}((p+q)^2, q^2) = \iint ds_2 ds_1 \frac{\rho^{(\text{OPE})}(s_1, s_2)}{(s_1 - (p+q)^2)(s_2 - q^2)}, \quad (12)$$

where the involved dual spectral density $\rho^{(\text{OPE})}(s_1, s_2)$ refers to,

$$\rho^{(\text{OPE})}(s_1, s_2) \equiv \frac{1}{\pi^2} \text{Im}_{s_1} \text{Im}_{s_2} F^{(\text{OPE})}(s_1, s_2). \quad (13)$$

After performing the double Borel transformation with respect to the variables $(p+q)^2 \rightarrow M_1^2$ and $q^2 \rightarrow M_2^2$, which is a technique used to enhance the convergence and suppress the contributions from

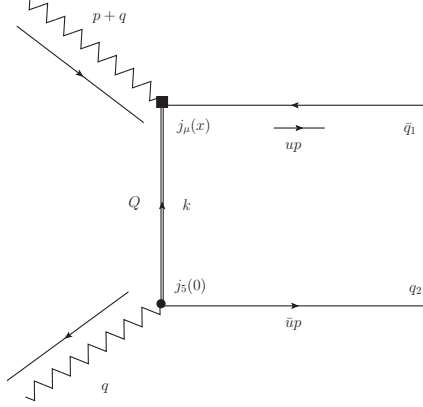


Figure 1: Diagrammatical representation of the leading-order (LO) contribution.

higher-dimensional operators in the operator product expansion (OPE), we arrive at the sum rules for the coupling constant g_{H^*HV} ,

$$f_H f_{H^*} g_{H^*HV} = -\frac{1}{m_H^2 m_{H^*}} \iint_{\tilde{\Sigma}} ds_2 ds_1 \exp\left(\frac{m_{H^*}^2 - s_1}{M_1^2} - \frac{m_H^2 - s_2}{M_2^2}\right) \rho^{(\text{OPE})}(s_1, s_2). \quad (14)$$

The inclusion of the integration boundary $\tilde{\Sigma}$, which is dual to the ground-state contribution to (10), arises from subtracting the continuum contributions using the parton-hadron duality ansatz.

3 Double spectral density of the correlation function

3.1 Double spectral density at LO

Near the light-cone, characterized by $x^2 \sim 0$, the OPE for the correlation function given in (8) remains applicable under the condition that both external momenta squared, $(p+q)^2$ and q^2 , are significantly below the heavy quark threshold m_Q^2 . Specifically, to ensure the validity of power counting within the OPE, it suffices to have:

$$m_Q^2 - q^2 \sim m_Q^2 - (p+q)^2 \sim \mathcal{O}(m_Q\tau), \quad n \cdot p \sim \mathcal{O}(m_Q). \quad (15)$$

Here, $\tau \gg \Lambda_{\text{QCD}}$ is a parameter independent of m_Q . The heavy quark propagating in the correlation function is consequently highly virtual and can be expanded near the light-cone. The initial expression in Eq. (8) undergoes transformation to:

$$F_\mu((p+q)^2, q^2) = -(m_Q + m_{q_2}) \int d^4x e^{-i(p+q)x} \langle V(p, \eta^*) | \bar{q}_1(x) \gamma_\mu S(x, 0) \gamma_5 q_2(0) | 0 \rangle, \quad (16)$$

where, $S_Q(x, 0)$ consists of the free-quark propagator and a term representing one-gluon emission, to our level of accuracy. Subsequently, we obtain the two-particle (2p) and three-particle (3p) contributions to the correlation function (16),

$$\begin{aligned}
F_{\mu,2p}^{(\text{LO})}((p+q)^2, q^2) &= \epsilon_{\mu\nu\rho\sigma} \eta^\nu p^\rho q^\sigma F_{2p}^{(\text{LO})}((p+q)^2, q^2) \\
&= -m_Q(1 + \hat{m}_{q_2}) \int d^4x \int \frac{d^4k}{(2\pi)^4} e^{-i(p+q+k)\cdot x} \langle V(p, \eta^*) | \bar{q}_1(x) \gamma_\mu \frac{i(\not{k} + m_Q)}{k^2 - m_Q^2} \gamma_5 q_2(0) | 0 \rangle, \\
F_{\mu,3p}^{(\text{LO})}((p+q)^2, q^2) &= \epsilon_{\mu\nu\rho\sigma} \eta^\nu p^\rho q^\sigma F_{3p}^{(\text{LO})}((p+q)^2, q^2) \\
&= ig_s m_Q(1 + \hat{m}_{q_2}) \int d^4x \int \frac{d^4k}{(2\pi)^4} e^{-i(k+p+q)\cdot x} \int_0^1 dv \langle V(p, \eta^*) | \bar{q}_1(x) \gamma_\mu \\
&\quad \times \left[\frac{\bar{v}(\not{k} + m_Q) \sigma_{\mu\nu} + v \sigma_{\mu\nu} (\not{k} + m_Q)}{2(k^2 - m^2)^2} \right] G^{\mu\nu}(vx) \gamma_5 q_2(0) | 0 \rangle. \tag{17}
\end{aligned}$$

Upon inserting the DAs into the correlation function, we focus on the key factors discussed below,

$$\begin{aligned}
\text{for two-particle case: } & \int_0^1 du \int \frac{d^4k}{(2\pi)^4} \int d^4x e^{-i(q+\bar{u}p+k)\cdot x}, \\
\text{for three-particle case: } & \int_0^1 du \int \frac{d^4k}{(2\pi)^4} \int d^4x e^{-i(q+\bar{\alpha}p+k)\cdot x}, \tag{18}
\end{aligned}$$

which reveal that for the two-particle case, $k \equiv -(q + \bar{u}p)$, with $\bar{u} = 1 - u$ and for the three-particle case, $k \equiv -(q + \bar{\alpha}p)$, with $\bar{\alpha} = 1 - \alpha = 1 - (\alpha_1 + v\alpha_3)$. The removal of the $1/px$ factors is accomplished by applying the replacement rules, as outlined below:

$$\begin{aligned}
\text{for two-particle case: } & \frac{1}{p \cdot x} \phi_{2p}(u) \rightarrow -i \int_0^u dz \phi_{2p}(z), \\
\text{for three-particle case: } & \frac{1}{p \cdot x} \Phi_{3p}(\underline{\alpha}) \rightarrow -i \hat{\Phi}_{3p}(\underline{\alpha}), \tag{19}
\end{aligned}$$

where the three-particle DAs with hat are defined as:

$$\hat{\Phi}_{3p}(\underline{\alpha}) \equiv \int_0^{\alpha_1} d\alpha'_1 \int_0^{1-\alpha'_1} d\alpha'_3 \delta(\alpha'_3 - \alpha_3) \Phi_{3p}(\alpha'_1, 1 - \alpha'_1 - \alpha_3, \alpha_3). \tag{20}$$

The LO results for the invariant amplitude are obtained by summing the contributions from individual twists up to twist-5 accuracy,

$$F^{(\text{LO})}((p+q)^2, q^2) = [F_{2p,tw2}^{(\text{LO})} + F_{2p,tw3}^{(\text{LO})} + F_{2p,tw4}^{(\text{LO})} + F_{2p,tw5}^{(\text{LO})} + F_{3p,tw4}^{(\text{LO})}]((p+q)^2, q^2). \tag{21}$$

For the three-particle case, a parallel expression is obtained by replacing $u(\bar{u})$ with $\alpha(\bar{\alpha})$. Consequently, we arrive at the following compact form through the power expansion:

$$F^{(\text{LO})}((p+q)^2, q^2) = \frac{1 + \hat{m}_{q_2}}{m_Q} \sum_{i=0}^4 \sum_{j=1}^4 \left\{ \int_0^1 du \delta_V^i \mathcal{C}^j(r_1, r_2, u) \mathcal{A}_{2p,ij}^{\text{LO}}(u) \right\}$$

$$+ \int_0^1 dv \int_0^1 d\alpha_1 \int_0^{1-\alpha_1} d\alpha_3 \delta_V^i \mathcal{C}^j(r_1, r_2, \alpha) \mathcal{A}_{3p, ij}^{\text{LO}}(v, \underline{\alpha}) \Big\}, \quad (22)$$

where $\delta_V = m_V/m_Q$, $\underline{\alpha} = (\alpha_1, \alpha_3)$, $\hat{m}_{q_2} = m_{q_2}^2/m_Q^2$,

$$\mathcal{C}(r_1, r_2, u) = \frac{1}{\bar{u}r_1 + ur_2 - 1}, \quad (23)$$

and $r_1 = (p+q)^2/m_Q^2$, $r_2 = q^2/m_Q^2$. The notations include:

$$\mathcal{A}_{2p, 01}^{\text{(LO)}}(u) = f_V^\perp \phi_{2;V}^\perp(u), \quad \mathcal{A}_{2p, 12}^{\text{(LO)}}(u) = -\frac{1}{2} f_V^\parallel \psi_{3;V}^\perp(u), \quad (24)$$

$$\mathcal{A}_{2p, 22}^{\text{(LO)}}(u) = \frac{f_V^\perp}{4} [4u\bar{u}\phi_{2;V}^\perp(u) + \phi_{4;V}^\perp(u)], \quad \mathcal{A}_{2p, 23}^{\text{(LO)}}(u) = -\frac{1}{2} f_V^\perp \phi_{4;V}^\perp(u), \quad (25)$$

$$\mathcal{A}_{2p, 33}^{\text{(LO)}}(u) = -f_V^\parallel u\bar{u}\psi_{3;V}^\perp(u), \quad \mathcal{A}_{2p, 34}^{\text{(LO)}}(u) = \frac{3}{4} f_V^\parallel \psi_{5;V}^\perp(u), \quad (26)$$

$$\mathcal{A}_{2p, 43}^{\text{(LO)}}(u) = \frac{f_V^\perp}{2} u\bar{u} [2u\bar{u}\phi_{2;V}^\perp(u) + \phi_{4;V}^\perp(u)], \quad \mathcal{A}_{2p, 44}^{\text{(LO)}}(u) = -\frac{3}{2} f_V^\perp u\bar{u}\phi_{4;V}^\perp(u), \quad (27)$$

$$\begin{aligned} \mathcal{A}_{3p, 22}^{\text{(LO)}}(v, \underline{\alpha}) &= f_V^\perp \left\{ 2\bar{v} [\Phi_{4;V}^{\perp(2)}(\underline{\alpha}) - \Phi_{4;V}^{\perp(1)}(\underline{\alpha})] - \Psi_{4;V}^\perp(\underline{\alpha}) - (v - \bar{v}) \tilde{\Psi}_{4;V}^\perp(\underline{\alpha}) \right. \\ &\quad \left. - \frac{2(v - \bar{v})}{\bar{\alpha}} [\widehat{\Phi}_{4;V}^{\perp(2)}(\underline{\alpha}) - \widehat{\Phi}_{4;V}^{\perp(1)}(\underline{\alpha}) + \widehat{\Phi}_{4;V}^{\perp(3)}(\underline{\alpha}) - \widehat{\Phi}_{4;V}^{\perp(4)}(\underline{\alpha})] \right\}, \end{aligned} \quad (28)$$

$$\mathcal{A}_{3p, 23}^{\text{(LO)}}(v, \underline{\alpha}) = f_V^\perp \frac{2(v - \bar{v})(r_2 - 1)}{\bar{\alpha}} [\widehat{\Phi}_{4;V}^{\perp(2)}(\underline{\alpha}) - \widehat{\Phi}_{4;V}^{\perp(1)}(\underline{\alpha}) + \widehat{\Phi}_{4;V}^{\perp(3)}(\underline{\alpha}) - \widehat{\Phi}_{4;V}^{\perp(4)}(\underline{\alpha})]. \quad (29)$$

Our next step is to derive the LO double spectral density, which is given by,

$$\rho^{\text{LO}}(s_1, s_2) = \frac{1}{\pi^2} \text{Im}_{s_1} \text{Im}_{s_2} F^{\text{(LO)}}((p+q)^2, q^2). \quad (30)$$

We extend the derivation of the dispersion representation within the framework of the tree-level factorization formula (21) by considering the general expression for double spectral densities governing invariant amplitudes in the two-particle case. The expression is given by,

$$\begin{aligned} \rho_{j, 2p}(s_1, s_2) &\equiv \frac{1}{\pi^2} \text{Im}_{s_1} \text{Im}_{s_2} \int_0^1 du \frac{\phi_{2p}(u)}{[\bar{u}s_1 + us_2 - m_Q^2 + i0]^j} \\ &= \frac{1}{\Gamma(j)} \frac{d^{j-1}}{(dm_Q^2)^{j-1}} \sum_k \frac{(-1)^{k+1} c_k^{(\phi_{2p})}}{\Gamma(k+1)} (s_1 - m_Q^2)^k \delta^{(k)}(s_1 - s_2) \\ &= \sum_k c_k^{(\phi_{2p})} \rho_{jk}(s_1, s_2), \end{aligned} \quad (31)$$

where the function $\phi_{2p}(u)$ is expressed through a Taylor expansion at $u = 0$

$$\phi_{2p}(u) = \sum_k c_k^{(\phi_{2p})} u^k. \quad (32)$$

The three-particle scenario follows a framework similar to that of the two-particle case,

$$\begin{aligned}
& \{\rho_{j,3p}(s_1, s_2), \widehat{\rho}_{j,3p}(s_1, s_2)\} \\
&= \frac{1}{\pi^2} \text{Im}_{s_1} \text{Im}_{s_2} \int_0^1 dv \int \mathcal{D}\alpha \frac{v^\ell \{\Phi_{3p}(\underline{\alpha}), \widehat{\Phi}_{3p}(\underline{\alpha})/\bar{\alpha}\}}{[\bar{\alpha} s_1 + \alpha s_2 - m_Q^2 + i0]^j} \\
&= \frac{1}{\Gamma(j)} \frac{d^{j-1}}{(dm_Q^2)^{j-1}} \frac{1}{\pi^2} \text{Im}_{s_1} \text{Im}_{s_2} \int_0^1 d\alpha \frac{\{\overline{\Phi}_{3p}(\alpha, \ell), \widehat{\overline{\Phi}}_{3p}(\alpha, \ell)\}}{\bar{\alpha} s_1 + \alpha s_2 - m_Q^2 + i0} \\
&= \frac{1}{\Gamma(j)} \frac{d^{j-1}}{(dm_Q^2)^{j-1}} \sum_k \frac{(-1)^{k+1} \{c_{\ell,k}^{\Phi_{3p}}, c_{\ell,k}^{\widehat{\Phi}_{3p}}\}}{\Gamma(k+1)} (s_1 - m_Q^2)^k \delta^{(k)}(s_1 - s_2) \\
&= \sum_k \{c_{\ell,k}^{\Phi_{3p}} \rho_{jk,3p}(s_1, s_2), c_{\ell,k}^{\widehat{\Phi}_{3p}} \widehat{\rho}_{jk,3p}(s_1, s_2)\}, \tag{33}
\end{aligned}$$

where the coefficient $c_{\ell,k}^{\Phi_{3p}}$ and $c_{\ell,k}^{\widehat{\Phi}_{3p}}$ originate from the series expansion of two “effective” DAs, namely $\overline{\Phi}_{3p}(\alpha, \ell)$, $\widehat{\overline{\Phi}}_{3p}(\alpha, \ell)$,

$$\begin{aligned}
\{\overline{\Phi}_{3p}(\alpha, \ell), \widehat{\overline{\Phi}}_{3p}(\alpha, \ell)\} &= \int_0^\alpha d\alpha_1 \int_{\alpha-\alpha_1}^{1-\alpha_1} d\alpha_3 \frac{(\alpha - \alpha_1)^\ell}{\alpha_3^{\ell+1}} \{\Phi_{3p}(\underline{\alpha}), \widehat{\Phi}_{3p}(\underline{\alpha})/\bar{\alpha}\} \\
&= \sum_k \{c_{\ell,k}^{\Phi_{3p}}, c_{\ell,k}^{\widehat{\Phi}_{3p}}\} \alpha^k, \quad \text{with } k \geq 2. \tag{34}
\end{aligned}$$

To account for the terms proportional to q^2 in Eq.(29), we introduce supplementary functions $\widetilde{\rho}_{jk,3p}(s_1, s_2)$ as described by Eq.(33):

$$\widetilde{\rho}_{jk,3p}(s_1, s_2) = s_2 \widehat{\rho}_{jk,3p}(s_1, s_2). \tag{35}$$

Performing a variable substitution by replacing α with u ,

$$\{\overline{\Phi}_{3p}(\alpha, \ell), \widehat{\overline{\Phi}}_{3p}(\alpha, \ell)\} \leftrightarrow \{\overline{\Phi}_{3p}(u, \ell), \widehat{\overline{\Phi}}_{3p}(u, \ell)\}, \tag{36}$$

facilitates the combination of contributions from three-particle processes with those from the previously considered two-particle contributions. With the replacement of each twist and multiplicity component in the sum (22) with its corresponding double dispersion form, we derive the LO double spectral density of the correlation function,

$$\begin{aligned}
\rho^{(\text{LO})}(s_1, s_2) &= m_Q(1 + \widehat{m}_{q_2}) \left\{ \rho_1^{(\phi_{2;V}^\perp)} + m_Q^2 \delta_V \rho_1^{(\psi_{3;V}^\perp)} \right. \\
&\quad \left. + m_Q^2 \delta_V^2 \left(\rho_2^{(\phi_{2;V}^\perp)} + \rho_1^{(\phi_{4;V}^\perp)} + \sum_{i=1}^2 \rho^{(\overline{\Phi}_{4;V}^\perp(i))} + m_Q^2 \rho_2^{(\phi_{4;V}^\perp)} \right) \right\}
\end{aligned}$$

$$\begin{aligned}
& + m_Q^2 \delta_V^2 \left[\rho^{(\bar{\Psi}_{4;V}^\perp)} + \rho^{(\bar{\Psi}_{4;V}^\perp)} + m_Q^2 \sum_{i=1}^4 \left(\rho^{(\bar{\Phi}_{4;V}^\perp(i))} + \tilde{\rho}^{(\bar{\Phi}_{4;V}^\perp(i))} \right) \right] \\
& + m_Q^4 \delta_V^3 \left(\rho_2^{(\psi_{3;V}^\perp)} + m_Q^2 \rho^{(\psi_{5;V}^\perp)} \right) \\
& + m_Q^4 \delta_V^4 \left[\left(\rho_3^{(\phi_{2;V}^\perp)} + \rho_3^{(\phi_{4;V}^\perp)} \right) + m_Q^2 \rho_4^{(\phi_{4;V}^\perp)} \right] \Big\} (s_1, s_2). \tag{37}
\end{aligned}$$

This expression features an expansion form (32) for each term, where the coefficients $c_k^{(\phi)}$ are readily determined from the polynomial form of the DAs, as explicitly presented in Appendix B. The resulting expression (37) contributes to a new and comprehensive understanding. For instance, we illustrate the contributions to $\rho^{(\text{LO})}$ from the twist-2 and twist-3 DAs, emphasizing their asymptotic behavior, with $\delta^{(k)}(x) \equiv d^k/dx^k[\delta(x)]$,

$$\begin{aligned}
\rho_1^{(\phi_{2;V}^\perp)}(s_1, s_2) &= 6f_V^\perp \left[(s_1 - m_Q^2) \delta^{(1)}(s_1 - s_2) + \frac{1}{2} (s_1 - m_Q^2)^2 \delta^{(2)}(s_1 - s_2) \right] \theta(s_2 - m_Q^2), \\
\rho_1^{(\psi_{3;V}^\perp)}(s_1, s_2) &= -3f_V^\parallel \frac{d}{dm_Q^2} \left[(s_1 - m_Q^2) \delta^{(1)}(s_1 - s_2) + \frac{1}{2} (s_1 - m_Q^2)^2 \delta^{(2)}(s_1 - s_2) \right] \theta(s_2 - m_Q^2), \\
\rho_2^{(\phi_{2;V}^\perp)}(s_1, s_2) &= -f_V^\perp \frac{d}{dm_Q^2} \left[3(s_1 - m_Q^2)^2 \delta^{(2)}(s_1 - s_2) + 2(s_1 - m_Q^2)^3 \delta^{(3)}(s_1 - s_2) \right. \\
&\quad \left. + \frac{1}{20} (s_1 - m_Q^2)^4 \delta^{(4)}(s_1 - s_2) \right] \theta(s_2 - m_Q^2), \\
\rho_2^{(\psi_{3;V}^\perp)}(s_1, s_2) &= \frac{1}{2} f_V^\parallel \frac{d^2}{d(m_Q^2)^2} \left[3(s_1 - m_Q^2)^2 \delta^{(2)}(s_1 - s_2) + 2(s_1 - m_Q^2)^3 \delta^{(3)}(s_1 - s_2) \right. \\
&\quad \left. + \frac{1}{20} (s_1 - m_Q^2)^4 \delta^{(4)}(s_1 - s_2) \right] \theta(s_2 - m_Q^2). \tag{38}
\end{aligned}$$

3.2 Double spectral density at NLO

To achieve next-to-leading order (NLO) precision, we express the invariant amplitude associated with the correlation function (8) in the following form,

$$F^{(\text{OPE})}((p+q)^2, q^2) = F^{(\text{LO})}((p+q)^2, q^2) + \frac{\alpha_s C_F}{4\pi} F^{(\text{NLO})}((p+q)^2, q^2). \tag{39}$$

The loop computations in this context closely follow the procedures detailed in [29] for the leading twist. The one-loop diagrams depicted in Figure 2 are computed using the method of regions, initially introduced in Ref. [46]. It is evident that only the hard region contributes significantly, while the

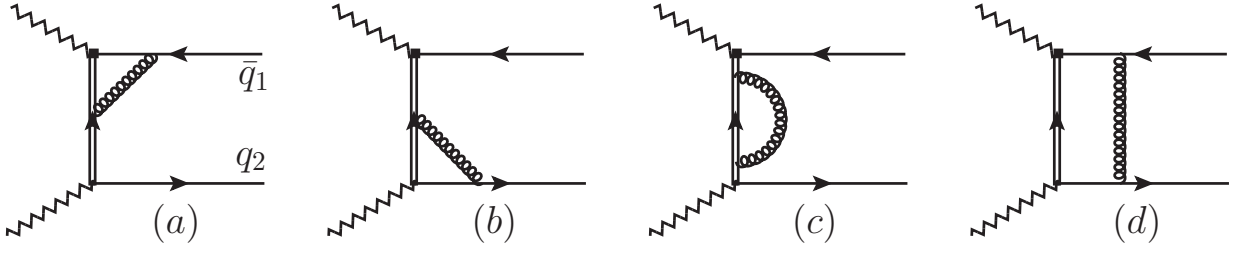


Figure 2: NLO QCD corrections of leading-twist contributions.

collinear region yields scaleless integrals within dimensional regularization, resulting in negligible contributions. The one-loop diagrams yield the following results:

$$\begin{aligned}
F_{H^*}^{(1),h}((p+q)^2, q^2) &= \frac{\alpha_s C_F}{4\pi} \left\{ \left[\frac{2(1-r_1)}{r_1-r_3} \ln \frac{1-r_3}{1-r_1} - 1 \right] \left[\frac{1}{\epsilon} + \ln \frac{\mu^2}{m_Q^2} - \ln \left[(1-r_3)(1-r_1) \right] \right] \right. \\
&\quad - \ln \left[(1-r_3)(1-r_1) \right] + \frac{1}{r_3-r_1} \left[2(1-r_1) (\text{Li}_2(r_3) - \text{Li}_2(r_1)) \right. \\
&\quad \left. \left. + \frac{(1-r_3)(1-r_3-2r_1)}{r_3} \ln(1-r_3) - \frac{(1-r_1)(1-3r_1)}{r_1} \ln(1-r_1) \right] - 4 \right\} F^{(0)}((p+q)^2, q^2), \\
F_H^{(1),h}((p+q)^2, q^2) &= -\frac{\alpha_s C_F}{4\pi} \left\{ 2 \left[\frac{1-r_2}{r_3-r_2} \ln \frac{1-r_3}{1-r_2} - 1 \right] \left[\frac{1}{\epsilon} + \ln \frac{\mu^2}{m_Q^2} - \ln \left[(1-r_3)(1-r_2) \right] \right] \right. \\
&\quad - 2 \ln \left[(1-r_3)(1-r_2) \right] - \frac{2}{r_3-r_2} \left[(1-r_2) (\text{Li}_2(r_3) - \text{Li}_2(r_2)) \right. \\
&\quad \left. \left. - \frac{(1-r_3)(1-r_3+r_2)}{r_3} \ln(1-r_3) + \frac{1-r_2}{r_2} \ln(1-r_2) \right] - 2 \right\} F^{(0)}((p+q)^2, q^2), \\
F_{wfc}^{(1)}((p+q)^2, q^2) &= -\frac{\alpha_s C_F}{4\pi} \left\{ \frac{7-r_3}{1-r_3} \left[\frac{1}{\epsilon} + \ln \frac{\mu^2}{m_Q^2} - \ln(1-r_3) + 1 \right] - \frac{1}{1-r_3} \left[\frac{1-7r_3}{r_3^2} \ln(1-r_3) \right. \right. \\
&\quad \left. \left. + \frac{1}{r_3} - 3 \right] \right\} F^{(0)}((p+q)^2, q^2). \tag{40}
\end{aligned}$$

Here, we introduce the definitions $r_1 \equiv (p+q)^2/m_Q^2$, and $r_2 \equiv q^2/m_Q^2$, with $r_3 = ur_2 + \bar{u}r_1$. The tree-level amplitude $F_\mu^{(0)}$ is presented at the leading twist,

$$F^{(0)}((p+q)^2, q^2) = (1 + \hat{m}_{q_2}) f_V^\perp(\mu) \int_0^1 du \mathcal{C}(r_1, r_2, u) \cdot \phi_{2;V}^\perp(u, \mu). \tag{41}$$

The box diagram yields contributions at order $\mathcal{O}(\epsilon)$ in dimensional regularization, and therefore does not significantly contribute. This observation is consistent with previous findings [37, 47], which

demonstrate the vanishing of hard-collinear factorization for the one-loop box diagram in the context of hadronic photon correction. Combining the contributions from all one-loop diagrams, the results are in agreement with those presented in a previous study [29]:

$$\begin{aligned}
& \mathcal{T}^{(1)}(r_1, r_2, \mu) \\
&= \frac{\alpha_s C_F}{4\pi} \left\{ (-2) \left[\frac{1-r_1}{r_3-r_1} \ln \frac{1-r_3}{1-r_1} + \frac{1-r_2}{r_3-r_2} \ln \frac{1-r_3}{1-r_2} + \frac{3}{1-r_3} \right] \left(\frac{1}{\epsilon} + \ln \frac{\mu^2}{m_Q^2} \right) \right. \\
&+ 2 \left[\left(\frac{1-r_1}{r_3-r_1} + \frac{1-r_2}{r_3-r_2} \right) \text{Li}_2(r_3) - \frac{1-r_1}{r_3-r_1} \text{Li}_2(r_1) - \frac{1-r_2}{r_3-r_2} \text{Li}_2(r_2) \right] \\
&+ 2 \left[\left(\frac{1-r_1}{r_3-r_1} + \frac{1-r_2}{r_3-r_2} \right) \ln^2(1-r_3) - \frac{1-r_1}{r_3-r_1} \ln^2(1-r_1) - \frac{1-r_2}{r_3-r_2} \ln^2(1-r_2) \right] \\
&+ \left[\frac{1-r_3}{r_3} \left(\frac{1-r_3-2r_1}{r_3-r_1} - \frac{2(1-r_3+r_2)}{r_3-r_2} \right) + \frac{1-6r_3}{r_3^2} + 1 \right] \ln(1-r_3) + \frac{1-9r_3}{r_3(1-r_3)} \\
&\quad \left. - \frac{(1-r_1)(1-3r_1)}{r_1(r_3-r_1)} \ln(1-r_1) + \frac{2(1-r_2)}{r_2(r_3-r_2)} \ln(1-r_2) - 3 + 3 \ln \frac{\nu^2}{\mu^2} \right\}, \tag{42}
\end{aligned}$$

It is important to emphasize the clear distinction between the renormalization scale, denoted as ν , and the factorization scale, represented as μ .

Previous work [37] has demonstrated that the matrix element of the evanescent SCET operator, denoted as $\langle O_{E,\mu} \rangle^{(1)}$, vanishes at order $\mathcal{O}(\alpha_s)$ within the NDR scheme of γ_5 when considering hard-collinear factorization. This leads to the factorization formula for twist-2 contributions at next-to-leading order (NLO):

$$F^{(\text{NLO})}((p+q)^2, q^2) = (1 + \hat{m}_{q_2}) f_V^\perp(\mu) \int_0^1 du \mathcal{C}(r_1, r_2, u) \cdot \phi_{2;V}^\perp(u, \mu) \cdot \mathcal{T}^{(1)}(r_1, r_2, \mu). \tag{43}$$

Now, it is imperative to advance further and obtain the NLO double spectral density:

$$\rho^{\text{NLO}}(s_1, s_2) = \frac{1}{\pi^2} \text{Im}_{s_1} \text{Im}_{s_2} F^{(\text{NLO})}((p+q)^2, q^2). \tag{44}$$

For the NLO terms, we employ asymptotic vector meson DAs. This choice is justified by observing that at LO, the non-asymptotic contributions from Gegenbauer moments in the twist-2 DA (as described in Eq.(81)) constitute only a small percentage in the LCSR, assuming typical values for the moments a_2 and a_4 . Additionally, for the K^* particle, terms related to a_1 and a_3 vanish due to the $u = 1/2$ condition used in the calculation, effectively eliminating odd Gegenbauer terms. The additional $\mathcal{O}(\alpha_s)$ factor significantly suppresses these contributions, keeping them well below the uncertainties inherent in the sum rule.

4 Quark-hadron duality and sum rules

After computing the double spectral density (13), we obtain the expression,

$$\rho^{(\text{OPE})}(s_1, s_2) = \rho^{(\text{LO})}(s_1, s_2) + \frac{\alpha_s C_F}{4\pi} \rho^{(\text{NLO})}(s_1, s_2), \quad (45)$$

where the LO contribution is provided in (37), and the NLO part consists of the twist-2 contributions, as detailed in (96).

Following Ref. [9], we adopt a specific parameterization for the boundaries:

$$\left(\frac{s_1}{s_*}\right)^\alpha + \left(\frac{s_2}{s_*}\right)^\alpha \leq 1, \quad s_1, s_2 \geq m_Q^2. \quad (46)$$

We explore three different duality regions: the triangular region where $\alpha = 1$ and $s_* = 2s_0$, the concave region with $\alpha = \frac{1}{2}$ and $s_* = 4s_0$, and the convex region where $\alpha = 2$ and $s_* = \sqrt{2}s_0$. Our findings reveal that the terms containing $\delta(s_1 - s_2)$ and its derivatives contribute equally across all duality regions. Therefore, only NLO contributions not involving the delta-function or its derivatives are affected by the choice of region. However, most of the LO and the primary part of NLO contributions come from integrating over the diagonal interval, which remains consistent across all regions. Therefore, we opt for the most practical choice: the triangular region, where $s_1 + s_2 \leq 2s_0$. Returning to the LCSR Eq. (14), we then assume equal Borel parameters $M_1^2 = M_2^2 = 2M^2$. This allows us to rewrite the sum rule as:

$$f_H f_{H^*} g_{H^* HV} = \frac{1}{m_H^2 m_{H^*}} \exp\left(\frac{m_H^2 + m_{H^*}^2}{2M^2}\right) \left[\mathcal{F}^{(\text{LO})}(M^2, s_0) + \frac{\alpha_s C_F}{4\pi} \mathcal{F}^{(\text{NLO})}(M^2, s_0) \right]. \quad (47)$$

Here, we define the integral over the triangular region as follows:

$$\mathcal{F}(M^2, s_0) \equiv \int_{-\infty}^{\infty} ds_1 \int_{-\infty}^{\infty} ds_2 \theta(2s_0 - s_1 - s_2) \exp\left(-\frac{s_1 + s_2}{2M^2}\right) \rho(s_1, s_2). \quad (48)$$

Each DA, expressed through its Taylor expansion (32), decomposes the density ρ into individual terms. Importantly, within the context of the triangular duality region, the resulting expressions for the integrals $\mathcal{F}(M^2, s_0)$ can be universally formulated for any generic DA.

To achieve this, a variable transformation is applied to the integration variables in (48): $s_1 = s(1 - v)$ and $s_2 = sv$, or vice versa, $s = s_1 + s_2$ and $v = s_2/(s_1 + s_2)$. This transformation simplifies the difference $(s_1 - s_2) \rightarrow s(1 - 2v)$, allowing the integration of the $\delta(s_1 - s_2) = \delta(1 - 2v)/s$ functions and their derivatives over v . Simultaneously, the exponential factor in (48) becomes independent of v . This results in the Taylor expansion of an arbitrary DA $\phi(u)$ reducing to its value or its derivative at $u = 1/2$. This yields the following simplified expression:

$$\mathcal{F}_j(M^2, s_0) = \frac{1}{(j-1)!} \left\{ (-1)^j (M^2)^{2-j} \exp\left(-\frac{m_Q^2}{M^2}\right) + \delta_{j1} M^2 \exp\left(-\frac{s_0}{M^2}\right) \right\} \phi(u) \Big|_{u=\frac{1}{2}}, \quad (49)$$

$$\tilde{\mathcal{F}}_j^{(\phi)}(M^2, s_0) = -\frac{1}{2(j-1)!} \frac{d^{\ell-1}}{dm_Q^2 j^{-1}} \int_{2m_Q^2}^{2s_0} ds \exp\left(-\frac{s}{2M^2}\right) \left[u \left(\frac{s}{2} - m_Q^2\right) \phi'(u) + \frac{s}{2} \phi(u) \right] \Big|_{u=\frac{1}{2}}. \quad (50)$$

In the subsequent analysis, $\tilde{\mathcal{F}}_3$ stands out as the only contributor to the second term in (49).

$$\tilde{\mathcal{F}}_3^{(\phi)}(M^2, s_0) = \left\{ \frac{m_Q^2}{2M^2} \exp\left(-\frac{m_Q^2}{M^2}\right) \phi(u) + \frac{1}{2} \exp\left(-\frac{m_Q^2}{M^2}\right) [u \phi'(u) - \phi(u)] \right\} \Big|_{u=\frac{1}{2}}. \quad (51)$$

In conclusion, the LO part of the LCSR in (47) is derived as a linear combination of distinct contributions from individual DAs:

$$\mathcal{F}^{(\text{LO})}(M^2, s_0) = \mathcal{F}_{2p}^{(\text{LO})}(M^2, s_0) + \mathcal{F}_{3p}^{(\text{LO})}(M^2, s_0) + \tilde{\mathcal{F}}_{3p}^{(\text{LO})}(M^2, s_0), \quad (52)$$

$$\begin{aligned} \mathcal{F}_{2p}^{(\text{LO})}(M^2, s_0) = & -m_Q^3(1 + \hat{m}_{q_2}) \exp\left(-\frac{m_Q^2}{M^2}\right) \left\{ \left[1 - \exp\left(\frac{m_Q^2 - s_0}{M^2}\right) \right] f_V^\perp \frac{M^2}{m_Q^2} \phi_{2;V}^\perp(u) \right. \\ & + \frac{1}{2} \delta_V f_V^\parallel \psi_{3;V}^\perp(u) - \delta_V^2 \left[\frac{f_V^\perp}{4} (4u\bar{u}\phi_{2;V}^\perp(u) + \phi_{4;V}^\perp(u)) + \frac{m_Q^2}{4M^2} f_V^\perp \phi_{4;V}^\perp(u) \right] \\ & - \delta_V^3 \left[\frac{m_Q^2}{2M^2} f_V^\parallel u\bar{u}\psi_{3;V}^\perp(u) + \frac{1}{8} \frac{m_Q^4}{M^4} \delta_V^3 f_V^\parallel \psi_{5;V}^\perp(u) \right] \\ & \left. + \delta_V^4 \left[\frac{m_Q^2}{4M^2} f_V^\perp u\bar{u} (2u\bar{u}\phi_{2;V}^\perp(u) + \phi_{4;V}^\perp(u)) + \frac{m_Q^4}{4M^4} f_V^\perp u\bar{u}\phi_{4;V}^\perp(u) \right] \right\} \Big|_{u=\frac{1}{2}}, \quad (53) \end{aligned}$$

$$\begin{aligned} \mathcal{F}_{3p}^{(\text{LO})}(M^2, s_0) = & m_Q^3(1 + \hat{m}_{q_2}) \delta_V^2 f_V^\perp \left\{ \exp\left(-\frac{m_Q^2}{M^2}\right) \left[2(\overline{\Phi}_{4;V}^{\perp(2)}(u, \ell) \Big|_{\ell=1}^{\ell=0} - \overline{\Phi}_{4;V}^{\perp(1)}(u, \ell) \Big|_{\ell=1}^{\ell=0}) \right. \right. \\ & - \overline{\Psi}_{4;V}^\perp(u, \ell) \Big|_{\ell=0} - \overline{\Psi}_{4;V}^\perp(u, \ell) \Big|_{\ell=1} + \overline{\Psi}_{4;V}^\perp(u, \ell) \Big|_{\ell=1}^{\ell=0} \\ & \left. \left. - 2\overline{\Phi}_{4;V}^{\perp(2134)}(u, \ell) \Big|_{\ell=1} + 2\overline{\Phi}_{4;V}^{\perp(2134)}(u, \ell) \Big|_{\ell=1}^{\ell=0} \right] \right\} \Big|_{u=\frac{1}{2}} \\ & - \frac{m_Q^5(1 + \hat{m}_{q_2})}{M^2} \delta_V^2 f_V^\perp \left\{ \exp\left(-\frac{m_Q^2}{M^2}\right) \right. \\ & \left. \times \left[-\overline{\Phi}_{4;V}^{\perp(2134)}(u, \ell) \Big|_{\ell=1} + \overline{\Phi}_{4;V}^{\perp(2134)}(u, \ell) \Big|_{\ell=1}^{\ell=0} \right] \right\} \Big|_{u=\frac{1}{2}}, \end{aligned}$$

$$\begin{aligned} \tilde{\mathcal{F}}_{3p}^{(\text{LO})}(M^2, s_0) = & -\frac{m_Q^5(1 + \hat{m}_{q_2})}{2M^2} \delta_V^2 f_V^\perp \exp\left(-\frac{m_Q^2}{M^2}\right) \left\{ \left(\frac{m_Q^2}{M^2} - 1 \right) \right. \\ & \left. \times \left[\overline{\Phi}_{4;V}^{\perp(2134)}(u, \ell) \Big|_{\ell=1} - \overline{\Phi}_{4;V}^{\perp(2134)}(u, \ell) \Big|_{\ell=1}^{\ell=0} \right] \right\} \end{aligned}$$

$$+ \left(u \frac{\partial \overline{\Phi}_{4;V}^{\perp(2134)}}{\partial u} (u, \ell) \Big|_{\ell=1} - u \frac{\partial \overline{\Phi}_{4;V}^{\perp(2134)}}{\partial u} (u, \ell) \Big|_{\ell=1}^{\ell=0} \Big|_{u=\frac{1}{2}} \right), \quad (54)$$

where

$$\overline{\Phi}_{4;V}^{\perp(2134)}(u, \ell) = \overline{\Phi}_{4;V}^{\perp(2)}(u, \ell) - \overline{\Phi}_{4;V}^{\perp(1)}(u, \ell) + \overline{\Phi}_{4;V}^{\perp(3)}(u, \ell) - \overline{\Phi}_{4;V}^{\perp(4)}(u, \ell), \quad \delta_V = \frac{m_V}{m_Q}. \quad (55)$$

After comparing our results with those in Ref. [8], we find agreement in the two-particle components. However, discrepancies arise in the three-particle counterparts, with numerical values displaying opposite signs. Upon careful examination, we identify a confusion in the simplification process observed in Eq. (25) of [8] (also referred to in Eqs. (4.10-4.16) of [29]). This confusion stems from overlooking the introduction of additional variables, as demonstrated in Eq. (20), when addressing three-particle expressions. Consequently, inaccuracies occur in integrating when applying the $1/p_x$ replacement rule to the three-particle DAs. Our discovery emphasizes the critical importance of accurately managing higher-order terms and highlights the necessity for validation and verification in theoretical frameworks.

The subsequent stage of our analysis involves deriving the NLO contribution to Eq. (47) by incorporating the twist-2 NLO double spectral densities, $\rho^{(\text{tw}2, \text{NLO})}(s_1, s_2)$, as explained in Eq. (96) of Appendix C. The resulting expression for $\mathcal{F}^{(\text{NLO})}(M^2, s_0)$ within the triangular duality region is presented below, capturing the higher-order corrections to the LCSR formulation.

$$\mathcal{F}^{(\text{NLO})}(M^2, s_0) = f_V^\perp m_Q^2 (1 + \hat{m}_{q_2}) \int_{2m_Q^2}^{2s_0} ds \exp\left(-\frac{s}{2M^2}\right) f^{(\text{tw}2)}\left(\frac{s}{m_Q^2} - 2\right), \quad (56)$$

accompanied by the NLO contributions of twist-2,

$$\begin{aligned} f^{(\text{tw}2)}(\sigma) = & 3 \left\{ \ln\left(\frac{\mu^2}{m_Q^2}\right) + \frac{3}{4} \ln\left(\frac{\nu^2}{\mu^2}\right) - \text{Li}_2(-\sigma) - \text{Li}_2(-\sigma - 1) + 2 \text{Li}_2\left(-\frac{\sigma}{2}\right) + \frac{\pi^2}{12} \right. \\ & + \ln\left(\frac{\sigma}{2}\right) \ln\left(\frac{\sigma+2}{2}\right) - \ln(\sigma+1) \ln(\sigma+2) + \frac{2(\sigma+1)^2}{(\sigma+2)^3} \ln(\sigma+1) \\ & \left. - \frac{7\sigma^3 + 50\sigma^2 + 100\sigma + 64}{4(\sigma+2)^3} \ln\left(\frac{\sigma}{2}\right) - \frac{1}{2} \ln\left(\frac{\sigma+2}{2}\right) - \frac{11\sigma^2 + 28\sigma + 24}{8(\sigma+2)^2} \right\}. \quad (57) \end{aligned}$$

It's important to note that the twist-2 part of the expression precisely matches that derived in [29]. When transitioning to the pole-mass scheme for the heavy quark, we incorporate the terms $\Delta f^{(\text{tw}2)}(\sigma)$ from (100) to (57). Additionally, we have verified the factorization-scale independence for both twist-2 terms in the LCSR (47) at $O(\alpha_s^2)$ in the asymptotic limit, which further enhances our confidence in the obtained results.

The derivation of the LCSR expression (47) for the strong H^*HV coupling, applicable to both $B_{(s)}$ and $D_{(s)}$ mesons with their respective b or c quark masses, is now complete for the triangular

duality region. This comprehensive formulation includes both LO and NLO terms, as described in (52) and (56), respectively. The formulation is now prepared for numerical analysis.

5 Numerical analysis

This section is dedicated to determining various input parameters and extracting the strong couplings $g_{D_{(s)}^* D_{(s)} V}$ and $g_{B_{(s)}^* B_{(s)} V}$ from the established LCSRs in Eq.(47). The mass of have-light mesons and light vector mesons are taken from the PDG [48]. The consideration of decay constants related to pseudoscalar and vector heavy-light mesons requires careful attention. We employ two distinct methods: the first utilizes LQCD values for decay constants of charmed and bottom mesons. Specifically, we incorporate $N_f = 2 + 1 + 1$ results from [49] for heavy pseudoscalar mesons and decay constant ratios from [43]

$$\begin{aligned}
f_D &= 212.0 \pm 0.7 \text{ MeV}, & f_B &= 190.0 \pm 1.3 \text{ MeV}, \\
f_{D_s} &= 249.9 \pm 0.5 \text{ MeV}, & f_{B_s} &= 230.3 \pm 1.3 \text{ MeV}, \\
f_{D^*} &= 228.5 \pm 7.7 \text{ MeV}, & f_{B^*} &= 182.02 \pm 4.4 \text{ MeV}, \\
f_{D_s^*} &= 271.6 \pm 5.0 \text{ MeV}, & f_{B_s^*} &= 224.3 \pm 2.6 \text{ MeV}.
\end{aligned} \tag{58}$$

For comparison, the second employs two-point QCD sum rules to determine decay constants f_H and f_{H^*} , ($H = D_{(s)}, B_{(s)}$), as described in [9, 42]. This approach incorporates NLO corrections to partially cancel the perturbative effects of the LCSRs. Here, we present the decay constant values computed using the two-point QCDSRs

$$\begin{aligned}
f_D &= 190.4_{-7.9}^{+8.9} \text{ MeV}, & f_B &= 201.1_{-17.6}^{+21.2} \text{ MeV}, \\
f_{D^*} &= 245.5_{-21.3}^{+24.1} \text{ MeV}, & f_{B^*} &= 214.2_{-17.8}^{+10.1} \text{ MeV}. \\
f_{D_s} &= 200.7_{-8.7}^{+10.4} \text{ MeV}, & f_{B_s} &= 223.2_{-18.0}^{+22.2} \text{ MeV}, \\
f_{D_s^*} &= 281.1_{-20.9}^{+24.6} \text{ MeV}, & f_{B_s^*} &= 245.2_{-25.3}^{+18.9} \text{ MeV}.
\end{aligned} \tag{59}$$

Here, we use the RunDec Mathematica package [41] to investigate the evolution of the QCD coupling and quark mass (in the $\overline{\text{MS}}$ scheme) with four-loop precision, as outlined in Table 1. Starting with initial conditions set at $m_Z = 91.1876$ GeV, we determine the running parameters. Matching scales are identified at 4.2 GeV for the transition from $n_f = 5$ to $n_f = 4$ and at 1.3 GeV for the transition from $n_f = 4$ to $n_f = 3$.

parameter	input value	[Ref.]	rescaled values
$\alpha_s(m_Z)$	0.1179 ± 0.0010		$\alpha_s(1.5 \text{ GeV}) = 0.34867^{+0.0102}_{-0.0097}$ $\alpha_s(3.0 \text{ GeV}) = 0.2527^{+0.0050}_{-0.0048}$
$\bar{m}_c(\bar{m}_c)$	$1.280 \pm 0.025 \text{ GeV}$	[48]	$\bar{m}_c(1.5 \text{ GeV}) = 1.205 \pm 0.034 \text{ GeV}$
$\bar{m}_b(\bar{m}_b)$	$4.18 \pm 0.03 \text{ GeV}$		$\bar{m}_b(3.0 \text{ GeV}) = 4.473 \pm 0.04 \text{ GeV}$
$(\bar{m}_u + \bar{m}_d)(2 \text{ GeV})$	$6.78 \pm 0.08 \text{ MeV}$	[48, 49]	$(\bar{m}_u + \bar{m}_d)(1.5 \text{ MeV}) = 7.305 \pm 0.09 \text{ MeV}$ $(\bar{m}_u + \bar{m}_d)(3.0 \text{ GeV}) = 6.331 \pm 0.07 \text{ MeV}$
$(\bar{m}_s)(2 \text{ GeV})$	$93.1 \pm 0.6 \text{ MeV}$	[48, 49]	$(\bar{m}_s)(1.5 \text{ MeV}) = 100.305 \pm 0.646 \text{ MeV}$ $(\bar{m}_s)(3.0 \text{ GeV}) = 86.936 \pm 0.560 \text{ MeV}$

Table 1: QCD parameters used in the LCSRs and two-point QCDSRs.

Our discussion for the vector meson LCDAs primarily focuses on the LO part of the sum rules in Eq.(52). As we explained in the last section, we need to determine the values of the DAs or their derivatives at the midpoint $u = 1/2$. This relies on a complete set of coefficients in the conformal expansion, which is shaped by the inherent symmetry properties governed by the renormalization group (RG) equation controlling their scale dependence [50]. It differs from the LCSRs for $B_{(s)} \rightarrow V$ and $D_{(s)} \rightarrow V$ form factors, where vector meson DAs undergo weighting by the Borel exponent and integration over a duality interval. Additionally, since we consider the NLO for asymptotic twist-2 two-particle DAs, the renormalization of Gegenbauer coefficients should extend up to NLO as well. This involves a complex multiplicative process, as illustrated by Eq.(83) in Appendix B.

In addition to the decay constants $f_V^{\perp,\parallel}(\mu)$ and twist-2 parameters $a_n^{\perp,\parallel}(\mu)$ detailed in Table 2, we present the Gegenbauer moments for the twist-3 and twist-4 DAs of vector mesons in Table 3. These DAs are developed up to the NLO of conformal expansion in Ref. [51, 52]. The normalization and non-asymptotic coefficients at $\mu = 1 \text{ GeV}$, used as input parameters, are determined through computations using QCD sum rules (see Ref. [51–53] and citations therein). For the ω meson, the decay constants $f_\omega^{\parallel} = 197(8) \text{ MeV}$ and $f_\omega^{\perp} = 148(13) \text{ MeV}$ are extracted from the provided reference [28]. The remaining parameters for this meson are consistent with those employed for the ρ meson.

Subsequently, we specify the renormalization scale of the quark-gluon coupling and quark masses, the factorization scale, the Borel parameters, and the quark-hadron duality thresholds of the LCSR in Eq.(47). These parameters play crucial role in determining the behavior of the sum rules and extracting the strong couplings. We choose these parameters to ensure that the sum rules exhibit strong convergence and stability, while also minimizing theoretical uncertainties in the final out-

	ρ		K^*		ϕ	
	$\mu = 1.5 \text{ GeV}$	$\mu = 3 \text{ GeV}$	$\mu = 1.5 \text{ GeV}$	$\mu = 3 \text{ GeV}$	$\mu = 1.5 \text{ GeV}$	$\mu = 3 \text{ GeV}$
$f_V^\parallel [\text{MeV}]$	216(3)	216(3)	220(5)	220(5)	215(5)	215(5)
$f_V^\perp [\text{MeV}]$	158(9)	150(8)	177(9)	168(8)	178(9)	169(8)
a_1^\parallel	0	0	0.027(18)	0.023(15)	0	0
a_1^\perp	0	0	0.036(27)	0.033(25)	0	0
a_2^\parallel	0.124(58)	0.100(47)	0.091(74)	0.073(60)	0.149(74)	0.120(60)
a_2^\perp	0.120(51)	0.101(43)	0.086(68)	0.072(58)	0.120(60)	0.101(51)

Table 2: Decay constants and twist-2 hadronic parameters, initially referenced at $\mu = 1 \text{ GeV}$ [53], are then scaled to $\mu = 1.5 \text{ GeV}$ and $\mu = 3 \text{ GeV}$ using the evolution equations outlined in Appendix B.

comes. Since we use the finite heavy quark mass, these parameters are naturally different for the couplings with charmed and bottom mesons. However, the heavy-quark spin symmetry enables certain scales and the Borel parameters to be aligned in the H and H^* channels. Detailed default values and intervals for these parameters are provided in Table 4, which offers a comprehensive overview of the specific values and intervals for the parameters mentioned above. The determination of the Borel parameter M^2 and the effective threshold s_0 in LCSRs follows established criteria aimed at ensuring the smallness of subleading power contributions in the light-cone OPE while simultaneously suppressing contributions from excited states. These criteria typically involve considerations of convergence and stability in the sum rule framework, and in our analysis, we adhere to them to ensure the reliability and accuracy of our results. These parameters, presented in Table 4, are consistent with prior choices in LCSR analyses of heavy-to-light decay form factors and couplings [9, 54, 55]. Additionally, we explore variations in the factorization scale μ within specified ranges for both charm-meson and bottom-meson couplings. This exploration allows us to assess the sensitivity of our results to variations in the factorization scale, providing valuable insights into the theoretical uncertainties associated with the factorization procedure. Furthermore, we maintain the renormalization scales of α_s and quark masses equal to the factorization scale μ used in the OPE. This choice is motivated by considerations of consistency within the theoretical framework and has been adopted in previous analyses within the field. By aligning these scales, we ensure coherence in our calculations and facilitate comparisons with prior studies.

Moreover, it's valuable to analyze how LCSR for $D_{(s)}^* D_{(s)} V$ and $B_{(s)}^* B_{(s)} V$ couplings, along with decay constant products, respond to changes in the Borel parameter M^2 and the scale μ . Figure 3 depicts the dependence on the Borel parameter M^2 , illustrating a nearly flat behavior within

	ρ		K^*		ϕ	
	$\mu = 1.5 \text{ GeV}$	$\mu = 3 \text{ GeV}$	$\mu = 1.5 \text{ GeV}$	$\mu = 3 \text{ GeV}$	$\mu = 1.5 \text{ GeV}$	$\mu = 3 \text{ GeV}$
ζ_{3V}^{\parallel}	0.022(7)	0.016(5)	0.017(6)	0.012(4)	0.018(6)	0.013(4)
$\tilde{\lambda}_{3V}^{\parallel}$	0	0	0.025(11)	0.017(7)	0	0
$\tilde{\omega}_{3V}^{\parallel}$	-0.059(19)	-0.037(12)	-0.046(19)	-0.028(12)	-0.030(10)	-0.019(6)
κ_{3V}^{\parallel}	0	0	0.000(1)	0.000(1)	0	0
ω_{3V}^{\parallel}	0.110(36)	0.078(24)	0.074(28)	0.052(19)	0.066(21)	0.046(15)
λ_{3V}^{\parallel}	0	0	-0.005(3)	-0.003(2)	0	0
κ_{3V}^{\perp}	0	0	0.003(3)	0.002(2)	0	0
ω_{3V}^{\perp}	0.435(198)	0.335(152)	0.237(79)	0.183(61)	0.158(63)	0.122(49)
λ_{3V}^{\perp}	0	0	-0.018(14)	-0.012(9)	0	0
ζ_{4V}^{\parallel}	0.062(27)	0.054(23)	0.018(18)	0.015(15)	0.000(18)	0.000(15)
$\tilde{\omega}_{4V}^{\parallel}$	-0.021(7)	-0.014(5)	-0.014(7)	-0.010(5)	-0.014(7)	-0.010(5)
ζ_{4V}^{\perp}	-0.026(41)	-0.022(32)	-0.009(24)	-0.008(19)	-0.009(24)	-0.008(19)
$\tilde{\zeta}_{4V}^{\perp}$	-0.065(41)	-0.052(32)	-0.041(32)	-0.032(26)	-0.025(32)	-0.020(26)
κ_{4V}^{\parallel}	0	0	-0.022(5)	-0.019(5)	0	0
κ_{4V}^{\perp}	0	0	0.012(5)	0.011(5)	0	0

Table 3: The twist-3 and twist-4 hadronic parameters, initially referenced at $\mu = 1 \text{ GeV}$ [53], are then scaled to $\mu = 1.5 \text{ GeV}$ and $\mu = 3 \text{ GeV}$ using the evolution equations outlined in Appendix B.

the range considered, indicating minimal sensitivity to variations in M^2 . This observation suggests that the extracted quantities are robust against changes in the Borel parameter, contributing to the reliability of our results. In Figure 4, we observe the dependence of individual contributions on the scale μ . Remarkably, contributions from twist-2 at both LO and NLO display significant but opposite dependencies on μ , almost canceling each other. While other higher-twist contributions exhibit minimal dependence, the overall outcome indicates only slight sensitivity to the scale μ . This behavior suggests a delicate balance between different contributions in the LCSRs framework, highlighting the importance of considering various factors when interpreting the results.

To ensure the efficiency of power corrections, we illustrate the contributions of each term in the power correction series, taking the heaviest ϕ meson as an example. From the Table 5, it is clear that for the D meson, despite the significant value of δ_ϕ , the contributions generally decrease in order of power. Contributions at δ_ϕ^1 and δ_ϕ^2 , compared to δ_ϕ^0 , are reduced by an order of magnitude, although

Parameter	default value (interval)	[Ref.]	Parameter	default value (interval)	[Ref.]
charmed meson sum rules			bottom meson sum rules		
μ (GeV)	1.5 (1.0-3.0)	[54]	μ (GeV)	3.0 (2.5-4.5)	[55]
M^2 (GeV ²)	4.5 (3.5-5.5)		M^2 (GeV ²)	16.0 (12.0-20.0)	
s_0 (GeV ²)	7.0 (6.5-7.5)		s_0 (GeV ²)	37.5 (35.0-40.0)	
\bar{M}^2 (GeV ²)	2.0 (1.5-2.5)	[42]	\bar{M}^2 (GeV ²)	5.5 (4.5-6.5)	[42]
\bar{s}_0 (GeV ²)	5.6 (f_D)		\bar{s}_0 (GeV ²)	33.9 (f_B)	
	6.3 (f_{D_s})			35.6(f_{B_s})	
\bar{s}_0^* (GeV ²)	6.2(f_{D^*})		\bar{s}_0^* (GeV ²)	34.1 (f_{B^*})	
	7.4 ($f_{D_s^*}$)		36.3 ($f_{B_s^*}$)		

Table 4: The renormalization scale μ , Borel parameters M^2 and \bar{M}^2 , along with duality thresholds s_0 and \bar{s}_0 (\bar{s}_0^*), are employed in the LCSR and the two-point QCDSRs to determine the decay constants of H (H^*) mesons for both charmed and bottom particles.

δ_ϕ^1 and δ_ϕ^2 exhibit similar magnitudes. Likewise, δ_ϕ^3 and δ_ϕ^4 , relative to δ_ϕ^2 and δ_ϕ^3 , are also suppressed by an order of magnitude, with δ_ϕ^2 and δ_ϕ^3 displaying comparable magnitudes. This pattern can be explained by noting that in Eq.(53), higher-power contributions are accompanied by a reduction in the ratio m_c^2/M^2 . In contrast to the D meson case, although the δ_ϕ for the B channel is much smaller, the ratio m_b^2/M^2 played a compensatory role, this leads to a similar power expansion behaviour for the $B_s^*B_s\phi$ coupling as the $D_s^*D_s\phi$.

We now explore the numerical effects of perturbative QCD and distinct higher-twist corrections on the products of strong couplings and decay constants computed in Eq.(47). The outcomes of individual twist and NLO effects are summarized in Table 6, along with relevant data uncertainties.

Power	δ_ϕ^0	δ_ϕ^1	δ_ϕ^2	δ_ϕ^3	δ_ϕ^4	total
$g_{D_s^*D_s\phi}$	2.41	0.63	-0.48	-0.045	0.020	2.54
$g_{B_s^*B_s\phi}$	2.47	0.53	-0.48	-0.016	0.020	2.86

Table 5: Power corrections for the strong couplings $g_{H^*H\phi}$ using the decay constants from LQCD, in units of [GeV⁻¹]. The expansion extends to the power of δ_ϕ ranging from 0 to 4, where $\delta_\phi = \delta_\phi^{(Q)} = m_\phi/m_Q$, for the coupling with $D_s^{(*)}$ meson $\delta_\phi^{(c)} = 0.85$ and for the coupling $B_s^{(*)}$ meson $\delta_\phi^{(b)} = 0.23$.

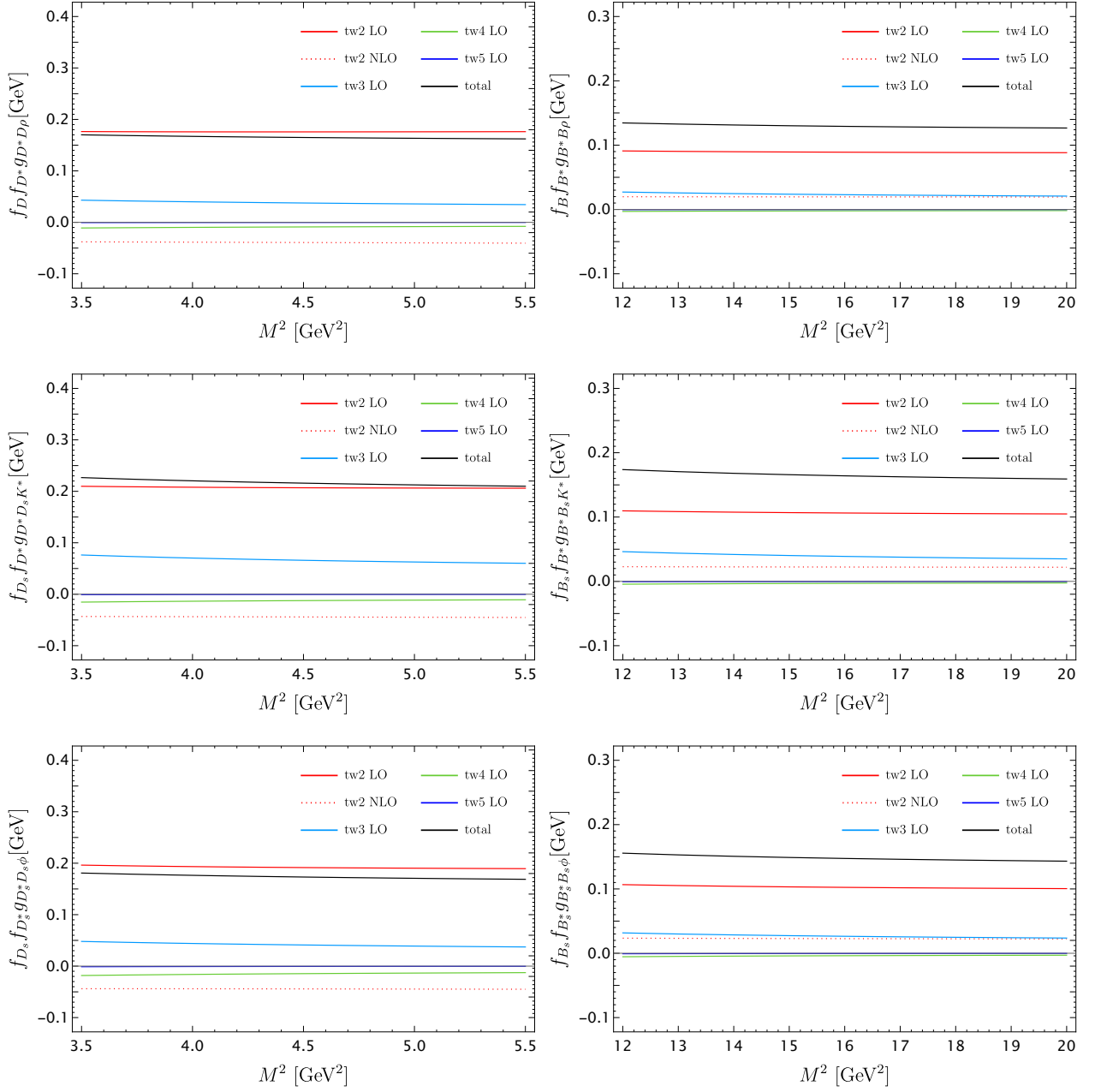


Figure 3: M^2 dependence of the products $f_{D^*} f_{D^{(s)}} g_{D^* D^{(s)} V}$ and $f_{B^*} f_{B^{(s)}} g_{B^* B^{(s)} V}$ calculated from LCSR. Displayed are the total values and separate contributions from twist-2 to twist-5 of the vector meson (ρ, K^*, ϕ) DAs, considering central values for all the other input parameters.

As observed in Table 6, the NLO corrections of twist-2 magnitude exhibit numerical equivalence with the LO contributions of twist-3, constituting roughly 20% of the leading twist for both charm and bottom scenarios. However, it's noteworthy that a sign difference is observed in NLO corrections of

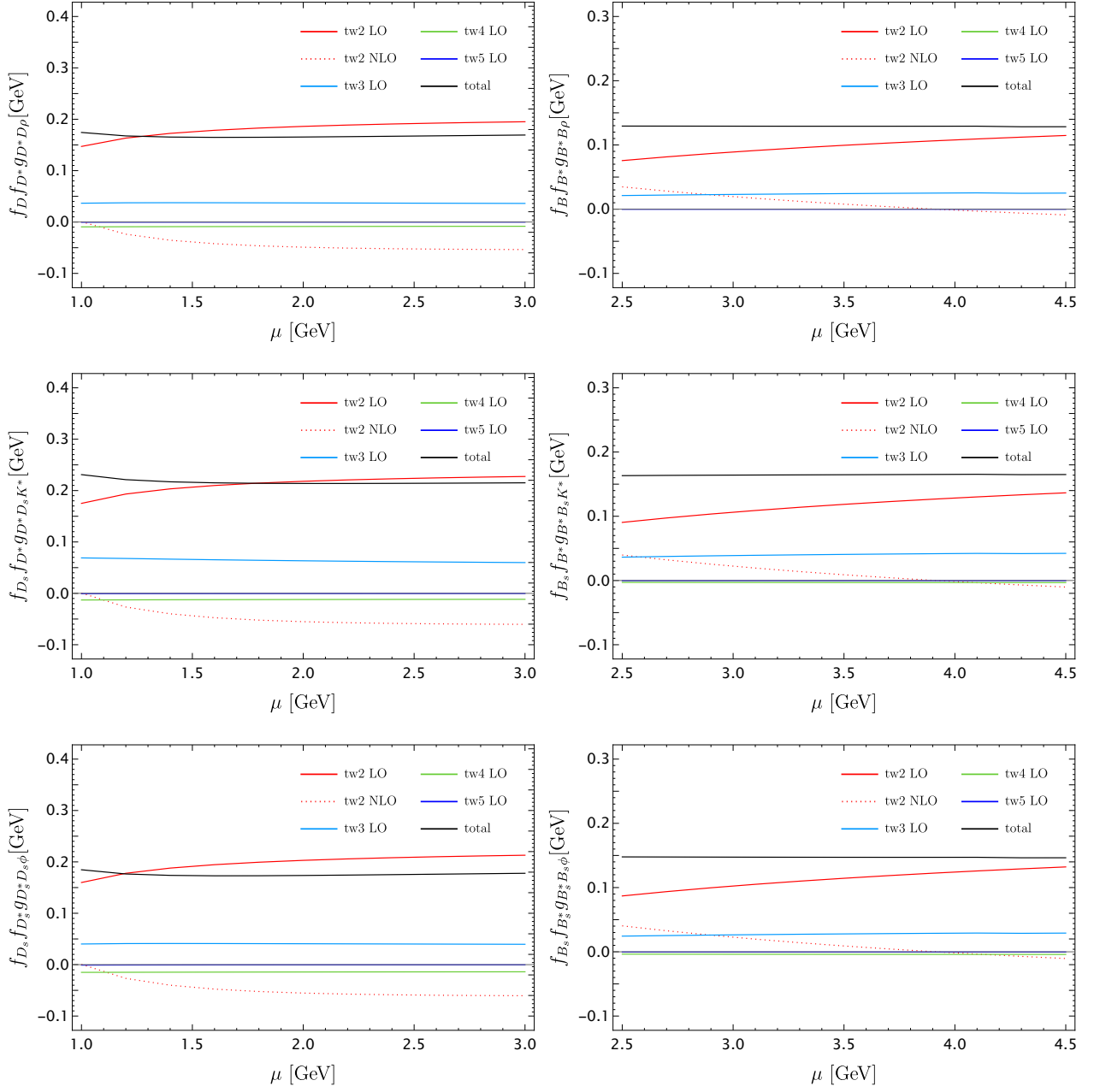


Figure 4: Scales dependence of the products $f_{D_{(s)}} f_{D_{(s)}} g_{D_{(s)} D_{(s)} V}$ and $f_{B_{(s)}} f_{B_{(s)}} g_{B_{(s)} B_{(s)} V}$ calculated from LCSR. Displayed are the total values and separate contributions from twist-2 to twist-5 of the vector meson(ρ, K^*, ϕ) DAs, considering central values for all other input parameters.

twist-2 between charm and bottom. This sign difference may arise from the difference in the scale ratio squared μ^2/m_Q^2 between charm and bottom systems, where $\mu^2/m_c^2 > 1$ for charm and $\mu^2/m_b^2 < 1$ for bottom, leading to distinct behaviors in the higher-order corrections. Additionally, our analysis

LCSR result	tw 2 LO	tw 2 NLO	tw 3 LO	tw 4 LO	tw 5 LO	total
$f_{D^*} f_D g_{D^* D \rho}$	$0.175^{+0.028}_{-0.036}$	$-0.039^{+0.041}_{-0.018}$	$0.038^{+0.006}_{-0.004}$	$-0.009^{+0.003}_{-0.003}$	$-0.0002^{+0.0001}_{-0.0003}$	$0.165^{+0.021}_{-0.022}$
$f_{D^*} f_D g_{D^* D \omega}$	$0.111^{+0.020}_{-0.024}$	$-0.025^{+0.026}_{-0.011}$	$0.024^{+0.004}_{-0.003}$	$-0.006^{+0.002}_{-0.002}$	$-0.0002^{+0.0001}_{-0.0002}$	$0.105^{+0.015}_{-0.015}$
$f_{D_s^*} f_D g_{D_s^* D K^*}$	$0.206^{+0.035}_{-0.043}$	$-0.044^{+0.046}_{-0.020}$	$0.041^{+0.007}_{-0.004}$	$-0.012^{+0.003}_{-0.004}$	$-0.0004^{+0.0002}_{-0.0004}$	$0.190^{+0.028}_{-0.029}$
$f_{D^*} f_{D_s} g_{D^* D_s K^*}$	$0.207^{+0.035}_{-0.043}$	$-0.044^{+0.046}_{-0.020}$	$0.041^{+0.007}_{-0.004}$	$-0.012^{+0.003}_{-0.004}$	$-0.0004^{+0.0002}_{-0.0005}$	$0.191^{+0.028}_{-0.029}$
$f_{D_s^*} f_{D_s} g_{D_s^* D_s \phi}$	$0.192^{+0.033}_{-0.041}$	$-0.044^{+0.046}_{-0.020}$	$0.041^{+0.007}_{-0.005}$	$-0.015^{+0.004}_{-0.005}$	$-0.0006^{+0.0003}_{-0.0007}$	$0.173^{+0.026}_{-0.027}$
$f_{B^*} f_B g_{B^* B \rho}$	$0.089^{+0.028}_{-0.018}$	$0.020^{+0.015}_{-0.029}$	$0.023^{+0.005}_{-0.003}$	$-0.002^{+0.001}_{-0.001}$	$-0.0002^{+0.0001}_{-0.0002}$	$0.129^{+0.013}_{-0.013}$
$f_{B^*} f_B g_{B^* B \omega}$	$0.056^{+0.018}_{-0.012}$	$0.012^{+0.010}_{-0.020}$	$0.015^{+0.003}_{-0.002}$	$-0.001^{+0.001}_{-0.001}$	$-0.0001^{+0.0001}_{-0.0001}$	$0.082^{+0.009}_{-0.009}$
$f_{B_s^*} f_B g_{B_s^* B K^*}$	$0.106^{+0.033}_{-0.022}$	$0.022^{+0.018}_{-0.033}$	$0.026^{+0.006}_{-0.003}$	$-0.003^{+0.001}_{-0.001}$	$-0.0002^{+0.0001}_{-0.0003}$	$0.151^{+0.017}_{-0.017}$
$f_{B^*} f_{B_s} g_{B^* B_s K^*}$	$0.106^{+0.034}_{-0.022}$	$0.022^{+0.018}_{-0.033}$	$0.026^{+0.006}_{-0.003}$	$-0.003^{+0.001}_{-0.002}$	$-0.0003^{+0.0001}_{-0.0003}$	$0.151^{+0.017}_{-0.017}$
$f_{B_s^*} f_{B_s} g_{B_s^* B_s \phi}$	$0.102^{+0.033}_{-0.021}$	$0.023^{+0.018}_{-0.033}$	$0.026^{+0.006}_{-0.004}$	$-0.004^{+0.001}_{-0.002}$	$-0.0004^{+0.0002}_{-0.0004}$	$0.147^{+0.016}_{-0.015}$

Table 6: Summary of the contribution from individual twist and NLO effects on the products of the strong couplings g_{H^*HV} and decay constants presented with both central values and associated data errors in units of [GeV].

indicates that the twist-5 contribution in the OPE of the correlation function has negligible impact, as validated through numerical assessments. This observation suggests that higher-order contributions beyond twist-4 have minimal influence on the computed results. Furthermore, the total uncertainty reported in Table 6 should involve variations stemming from changes in the duality region within the NLO aspect. Specifically, for the charm scenario, this variation amounts to around 20%, while for the bottom scenario, it stands at approximately 15%. These variations are reflected in the parameter $\Delta\alpha$, as depicted in Tables 8 and 9, where α is defined in Eq. (46). It's suggested that these uncertainties, to some extent, address the ‘‘systematic error’’ inherent in the quark-hadron duality ansatz applied in LCSRs.

In our final analysis, we normalize the couplings using heavy meson decay constants by two methods: the two-point QCDSRs in Eq.(59) and LQCD results in Eq.(58). Table 7 highlights the main findings, while Tables 8 and 9 provide more details on the parameters for each set of decay constants. In the D meson sector, the main sources of uncertainty lie in the Gegenbauer moment a_2^\perp and tensor decay constants f_V^\perp derived from LQCD. When employing two-point sum rules to calculate decay constants, an additional uncertainty arises from the decay constant itself, which is comparable in magnitude. In the B meson sector, the uncertainties related to the Borel parameter and threshold somehow increase relative to those in the D meson sector.

The estimation for the $D_{(s)}^* D_{(s)} V$ and $B_{(s)}^* B_{(s)} V$ strong couplings from LCSRs yields uncertainty

	decay constants	$g_{D^*D\rho}$	$g_{D^*D\omega}$	$g_{D_s^*DK^*}$	$g_{D^*D_sK^*}$	$g_{D_s^*D_s\phi}$
Charm	two-point QCDSRs	$3.53^{+0.61}_{-0.57}$	$2.25^{+0.42}_{-0.41}$	$3.55^{+0.65}_{-0.61}$	$3.87^{+0.73}_{-0.68}$	$2.69^{+0.55}_{-0.52}$
	LQCD	$3.40^{+0.49}_{-0.43}$	$2.17^{+0.34}_{-0.32}$	$3.30^{+0.52}_{-0.48}$	$3.34^{+0.54}_{-0.53}$	$2.54^{+0.40}_{-0.39}$
	decay constants	$g_{B^*B\rho}$	$g_{B^*B\omega}$	$g_{B_s^*BK^*}$	$g_{B^*B_sK^*}$	$g_{B_s^*B_s\phi}$
bottom	two-point QCDSRs	$3.00^{+0.49}_{-0.44}$	$1.88^{+0.34}_{-0.30}$	$3.12^{+0.60}_{-0.50}$	$3.16^{+0.52}_{-0.47}$	$2.70^{+0.49}_{-0.41}$
	LQCD	$3.74^{+0.38}_{-0.38}$	$2.38^{+0.28}_{-0.28}$	$3.61^{+0.40}_{-0.39}$	$3.61^{+0.41}_{-0.40}$	$2.86^{+0.32}_{-0.30}$

Table 7: LCSR results for the strong couplings g_{H^*HV} for the two methods of dividing out the decay constants in units of $[\text{GeV}^{-1}]$.

ranges of 13% to 18% and 10% to 18%, respectively, when using heavy-meson decay constants from the two-point QCDSRs. These uncertainty intervals are calculated based on variations in the input parameters and methodologies used in the LCSR analysis. While the uncertainty intervals for $g_{D_{(s)}^*D_{(s)}V}$ remain consistent regardless of the decay constant choice, only slight agreement is observed in the intervals for $g_{B_{(s)}^*B_{(s)}V}$. The difference in the central values of the $B_{(s)}^*B_{(s)}V$ couplings mainly arise from a 20% discrepancy between the lattice-QCD value of $f_{B_{(s)}^*}$ and the central value predicted by the two-point sum rule. For consistency, we use the two-point QCDSRs at NLO, with more precise sum rules at NNLO [42], yielding results consistent with LQCD calculations within uncertainties. This ensures that our analysis incorporates the latest advancements in theoretical frameworks and maintains consistency with the most accurate calculations available.

To investigate the $SU(3)_F$ symmetry breaking effects, we introduce Δr_{H^*HV} as the parameter characterizing the size of the breaking effects,

$$\Delta r_{D_{(s)}^*D_{(s)}V} = \frac{C_V \cdot g_{D_{(s)}^*D_{(s)}V} - g_{D^*D\rho}}{g_{D^*D\rho}}, \quad \Delta r_{B_{(s)}^*B_{(s)}V} = \frac{C_V \cdot g_{B_{(s)}^*B_{(s)}V} - g_{B^*B\rho}}{g_{B^*B\rho}}, \quad (60)$$

where $g_{D^*D\rho}$ and $g_{B^*B\rho}$ are defined in Eq.(4) and (5), respectively. Additionally, $C_V = \sqrt{2}$ for V takes the ω meson, otherwise, it's set to 1.

In Table 10, we detail the relative magnitudes of $SU(3)_F$ symmetry breaking effects for the various strong couplings. Interestingly, both $\Delta r_{D^*D\omega}$ and $\Delta r_{B^*B\omega}$ remain constant at -10% . This stability is attributed to the interplay of specific factors such as f_ω^\perp , f_ω^\parallel , and m_ω , which decrease at rates of 8%, 1.9%, and 0.1%, respectively. The other parameters remain consistent with those associated with the ρ meson, resulting in a cancellation of terms in both the numerator and denominator. Shifting focus to the 9.8% breaking observed in $\Delta r_{D^*D_sK^*}$, analysis using the decay constants from two-point QCDSRs reveals four primary sources of this deviation. Firstly, a substantial 12% deviation arises from the LCDAs of the K^* meson (8%) and the effect of the light quark mass (4%). Secondly, the

	central value	Δf_H	Δf_{H^*}	$\Delta\mu$	Δm_Q	Δs_0	ΔM^2	Δf_V^\perp	Δa_2^\perp	$\Delta\alpha$	Δ_{tot}
$g_{D^*D\rho}$	3.53	+0.15 -0.15	+0.33 -0.32	+0.20 -0.01	+0.07 -0.08	+0.06 -0.06	+0.11 -0.06	± 0.14	± 0.35	± 0.17	+0.61 -0.57
	3.40	+0.01 -0.01	+0.11 -0.11	+0.19 -0.01	+0.07 -0.07	+0.06 -0.08	+0.10 -0.06	± 0.14	± 0.34	± 0.16	+0.49 -0.43
$g_{D^*D\omega}$	2.25	+0.10 -0.10	+0.21 -0.20	+0.13 -0.01	+0.04 -0.05	+0.04 -0.05	+0.07 -0.04	± 0.15	± 0.22	± 0.15	+0.42 -0.41
	2.17	+0.01 -0.01	+0.08 -0.07	+0.12 -0.01	+0.04 -0.05	+0.04 -0.05	+0.07 -0.04	± 0.14	± 0.21	± 0.15	+0.34 -0.32
$g_{D_s^*DK^*}$	3.55	+0.15 -0.16	+0.29 -0.29	+0.20 -0.03	+0.06 -0.07	+0.07 -0.09	+0.13 -0.07	± 0.13	± 0.45	± 0.16	+0.65 -0.61
	3.30	+0.01 -0.01	+0.06 -0.06	+0.18 -0.01	+0.06 -0.07	+0.07 -0.08	+0.12 -0.07	± 0.12	± 0.42	± 0.15	+0.52 -0.48
$g_{D^*D_sK^*}$	3.87	+0.18 -0.19	+0.37 -0.35	+0.21 -0.03	+0.07 -0.07	+0.08 -0.10	+0.14 -0.08	± 0.14	± 0.49	± 0.18	+0.73 -0.68
	3.34	+0.01 -0.01	+0.12 -0.11	+0.19 -0.03	+0.06 -0.06	+0.07 -0.09	+0.12 -0.07	± 0.12	± 0.42	± 0.15	+0.54 -0.53
$g_{D_s^*D_s\phi}$	2.69	+0.14 -0.15	+0.25 -0.25	+0.17 -0.01	+0.06 -0.06	+0.06 -0.08	+0.13 -0.08	± 0.11	± 0.37	± 0.16	+0.55 -0.52
	2.54	+0.01 -0.01	+0.05 -0.05	+0.14 -0.01	+0.05 -0.05	+0.05 -0.06	+0.11 -0.06	± 0.09	± 0.31	± 0.13	+0.40 -0.39

Table 8: Summary of the individual uncertainties for the strong couplings g_{H^*HV} predicted from the LCSR (47) in units of $[\text{GeV}^{-1}]$. The negligible uncertainties arising from variations in the remaining input parameters have been considered but are not explicitly enumerated here, but are already taken into account in the determinations of the total errors.

decay constants of the D_s meson contribute approximately -5% . Thirdly, the decay constant $f_{K^*}^\perp$ explains 9% of the observed breaking. Lastly, the mass of the D_s meson contributes roughly -6% . As for $\Delta r_{D_s^*DK^*}$, the contribution from the D_s meson's decay constant $f_{D_s^*}$ is around -12.9% , larger than that of D_s . Additionally, a portion of this difference can be attributed to the mass of the D_s^* meson, resulting in a decrease of about 0.27%. This results in an overall breaking of 7.6%. Substituting decay constants calculated via LQCD for those obtained from two-point QCDSRs notably alters the quantification of symmetry breaking effects, primarily reducing the attributed deviation from decay constants. It's crucial to highlight that the breaking effects observed in ϕ , as determined through LQCD, tends to exceed that calculated using two-point QCDSRs (taking their absolute magnitudes into account). This discrepancy arises from the substantial difference in the decay constant f_{D_s} obtained from the two methods, which causes the negative breaking effects up to 15% from LQCD, larger than 5% from the two-point QCDSRs. However, for $f_{D_s^*}$, the situation is reversed but less difference, -13% from two-point QCDSRs compared to -15% from LQCD. Consequently, the discrepancy attributed to LQCD calculated decay constants amounts to -25% , compared to -13% from two-point QCDSRs. Finally, after accounting for additional factors contributing around 5% to

	central value	Δf_H	Δf_{H^*}	$\Delta\mu$	Δm_Q	Δs_0	ΔM^2	Δf_V^\perp	Δa_2^\perp	$\Delta\alpha$	Δ_{tot}
$g_{B^*B\rho}$	3.00	± 0.29	$+0.27$ -0.14	$+0.01$ -0.02	$+0.04$ -0.04	$+0.15$ -0.18	$+0.12$ -0.06	± 0.13	± 0.16	± 0.07	$+0.49$ -0.44
	3.74	± 0.03	$+0.09$ -0.09	$+0.01$ -0.02	$+0.05$ -0.06	$+0.19$ -0.23	$+0.15$ -0.07	± 0.17	± 0.20	± 0.08	$+0.38$ -0.38
$g_{B^*B\omega}$	1.88	± 0.18	$+0.17$ -0.09	$+0.00$ -0.01	$+0.03$ -0.03	$+0.10$ -0.12	$+0.08$ -0.04	± 0.14	± 0.10	± 0.06	$+0.34$ -0.30
	2.38	± 0.02	$+0.06$ -0.06	$+0.01$ -0.02	$+0.03$ -0.04	$+0.12$ -0.15	$+0.10$ -0.05	± 0.17	± 0.13	± 0.08	$+0.28$ -0.28
$g_{B_s^*BK^*}$	3.12	± 0.30	$+0.36$ -0.22	$+0.01$ -0.01	$+0.05$ -0.05	$+0.16$ -0.20	$+0.15$ -0.08	± 0.12	± 0.21	± 0.08	$+0.60$ -0.50
	3.61	± 0.02	$+0.04$ -0.04	$+0.01$ -0.01	$+0.05$ -0.06	$+0.19$ -0.23	$+0.17$ -0.09	± 0.14	± 0.25	± 0.08	$+0.40$ -0.39
$g_{B^*B_sK^*}$	3.16	± 0.29	$+0.29$ -0.14	$+0.01$ -0.01	$+0.05$ -0.05	$+0.16$ -0.20	$+0.15$ -0.08	± 0.12	± 0.22	± 0.07	$+0.52$ -0.47
	3.61	± 0.02	$+0.09$ -0.09	$+0.01$ -0.01	$+0.05$ -0.06	$+0.18$ -0.23	$+0.17$ -0.09	± 0.14	± 0.25	± 0.08	$+0.41$ -0.40
$g_{B_s^*B_s\phi}$	2.70	± 0.24	$+0.31$ -0.19	$+0.01$ -0.01	$+0.04$ -0.04	$+0.14$ -0.17	$+0.15$ -0.08	± 0.10	± 0.17	± 0.06	$+0.49$ -0.41
	2.86	± 0.02	$+0.03$ -0.03	$+0.01$ -0.01	$+0.04$ -0.04	$+0.15$ -0.18	$+0.16$ -0.08	± 0.11	± 0.18	± 0.07	$+0.32$ -0.30

Table 9: Summary of the individual theory uncertainties for the strong couplings g_{H^*HV} predicted from the LCSR (47) in units of $[\text{GeV}^{-1}]$. The negligible uncertainties arising from variations in the remaining input parameters have been considered but are not explicitly enumerated here, but are already taken into account in the determinations of the total errors.

the observed symmetry breaking effects, we arrive at our comprehensive analysis of $SU(3)$ flavour symmetry deviations. The situation with $SU(3)$ symmetry breaking in the B sector resembles that in the D sector, albeit with milder decrease.

When comparing our numerical outcomes with those of Ref. [8], depicted in Tables 11 and 12, we observed a reduction of the reported values $3.80_{-0.45}^{+0.59} \text{GeV}^{-1}$ and $3.89_{-0.48}^{+0.52} \text{GeV}^{-1}$ for $g_{D^*D\rho}$ and $g_{B^*B\rho}$ respectively. The primary reason for this difference lies in variations in our chosen input parameters such as scale μ , Borel parameter M^2 , and effective threshold s_0 . The impact of the scale μ is especially pronounced in the twist-2 LO and NLO aspects, although its overall effect decreases. Shifting the scale in the bottom sector from $\mu = 3 \text{GeV}$ to $\mu = m_b$ leads to an opposite sign for the NLO terms. Moreover, their specified values of M^2 and s_0 differ from our using.² We also extend our analysis to include sub-subleading power corrections ranging from twist-3 to twist-5

²The authors in [8] specified $M^2 = 4.5 \pm 1.0 \text{GeV}^2$ for charm and $M^2 = 18 \pm 3.0 \text{GeV}^2$ for bottom sector, with $M_1^2 = M_2^2 = M^2$, whereas we used $M_1^2 = M_2^2 = 2M^2$ differing by a factor of 2. Their choices of $s_0 = 6.0 \pm 0.5 \text{GeV}^2$ for charm and $s_0 = 34.0 \pm 1.0 \text{GeV}^2$ for bottom sector contrast with our selections of $7.0 \pm 0.5 \text{GeV}^2$ and $37.5 \pm 2.5 \text{GeV}^2$, respectively.

$\Delta r_{D_{(s)}^* D_{(s)} V}$	decay constants	$\Delta r_{D^* D \omega}$	$\Delta r_{D_s^* DK^*}$	$\Delta r_{D^* D_s K^*}$	$\Delta r_{D_s^* D_s \phi}$
charm	two-point QCDSRs	-10%	7.6%	9.8%	-13%
	LQCD	-10%	-3%	-1.8%	-25%
$\Delta r_{B_{(s)}^* B_{(s)} V}$	decay constants	$\Delta r_{B^* B \omega}$	$\Delta r_{B_s^* BK^*}$	$\Delta r_{B^* B_s K^*}$	$\Delta r_{B_s^* B_s \phi}$
bottom	two-point QCDSRs	-10%	3.9%	5.4%	-9.9%
	LQCD	-10%	-3.5%	-3.5%	-23%

Table 10: Summary of the extent of $SU(3)$ breaking effects as determined by LCSR, with $\Delta r_{H^* HV}$ serving as a measurement parameter.

Method	$g_{D^* D \rho}$	$g_{D^* D \omega}$	$g_{D_s^* DK^*}$	$g_{D^* D_s K^*}$	$g_{D_s^* D_s \phi}$
LCSR[8]	$3.80^{+0.59}_{-0.45}$	–	–	–	–
LCSR[19]	3.56 ± 0.60	–	–	4.04 ± 0.8	3.28 ± 0.64
LCSR[17]	4.17 ± 1.04	–	–	–	–
QCDSR[21]	–	–	3.74 ± 1.38	–	–
LCSR (this work)	$3.53^{+0.61}_{-0.57}$	$2.25^{+0.42}_{-0.41}$	$3.55^{+0.65}_{-0.61}$	$3.87^{+0.73}_{-0.68}$	$2.69^{+0.55}_{-0.52}$
	$3.40^{+0.49}_{-0.43}$	$2.17^{+0.34}_{-0.32}$	$3.30^{+0.52}_{-0.48}$	$3.34^{+0.54}_{-0.53}$	$2.54^{+0.40}_{-0.39}$

Table 11: Numerical values of coupling $g_{D_{(s)}^* D_{(s)} V} (\text{GeV}^{-1})$ from several methods.

(considering δ_V^3 and δ_V^4) in Eq.(53), which were absent in [8]. Additionally, our treatment of the three-particle contributions deviates from that in [8] due to our modifications to the three-particle DAs, resulting in a reversal of signs, although their influence remains negligible compared to the leading twist contribution. Furthermore, it is noteworthy that the LCSR studies conducted in [17, 19] only focused on leading-order calculations, while the significant compensatory effects from the twist-2 NLO calculations were absent. As mentioned previously, in the case of charm mesons, the NLO effects at the leading twist effectively counterbalance the corrections from higher-twist contributions. Consequently, we expect our results to align closely with those from earlier sum rule investigations, within the errors. However, in the case of bottom mesons, the opposite sign of the NLO effects enhance the impact of the leading twist.

In addition, we introduce an alternative method to determine the $B_{(s)}^* B_{(s)} V$ coupling. This method, as extensively described in [8, 9], utilizes the hadronic dispersion relation for the $B_{(s)} \rightarrow V$

Method	$g_{B^*B\rho}$	$g_{B^*B\omega}$	$g_{B_s^*BK^*}$	$g_{B^*B_sK^*}$	$g_{B_s^*B_s\phi}$
LCSR[8]	$3.89^{+0.52}_{-0.48}$	–	–	–	–
LCSR[17]	5.70 ± 1.43	–	–	–	–
QCDSR[21]	–	–	3.24 ± 1.08	–	–
LCSR (this work)	$3.00^{+0.49}_{-0.44}$	$1.88^{+0.34}_{-0.30}$	$3.12^{+0.60}_{-0.50}$	$3.16^{+0.52}_{-0.47}$	$2.70^{+0.49}_{-0.41}$
	$3.74^{+0.38}_{-0.38}$	$2.38^{+0.28}_{-0.28}$	$3.61^{+0.40}_{-0.39}$	$3.61^{+0.41}_{-0.40}$	$2.86^{+0.32}_{-0.30}$

Table 12: Numerical values of coupling $g_{B_{(s)}^*B_{(s)}V}(\text{GeV}^{-1})$ from several methods.

vector(tensor) form factor as a foundational element:

$$V(q^2) = \frac{(m_{B_{(s)}} + m_V)g_{B_{(s)}^*B_{(s)}V}f_{B_{(s)}^*}}{2m_{B_{(s)}^*}(1 - q^2/m_{B_{(s)}^*}^2)} + \frac{1}{\pi} \int_{(m_{B_{(s)}} + m_V)^2}^{\infty} dt \frac{\text{Im}V(t)}{t - q^2}, \quad (61)$$

$$T_1(q^2) = \frac{g_{B_{(s)}^*B_{(s)}V}f_{B_{(s)}^*}^{\perp}}{2(1 - q^2/m_{B_{(s)}^*}^2)} + \frac{1}{\pi} \int_{(m_{B_{(s)}} + m_V)^2}^{\infty} dt \frac{\text{Im}T_1(t)}{t - q^2}. \quad (62)$$

This relation features the vector-meson $B_{(s)}^*$ pole, just below the kinematic threshold $q^2 = (m_{B_{(s)}} + m_V)^2$. The residue of the B^* pole represents the product of the $B_{(s)}^*B_{(s)}V$ coupling and the $B_{(s)}^{*(\perp)}$ decay constant. Multiplying both sides of Eq.(62) by the denominator of the pole term and taking the limit $q^2 \rightarrow m_{B_{(s)}^*}^2$, we avoid the integral over the hadronic spectral density, leading to:

$$g_{B_{(s)}^*B_{(s)}V} = \frac{2m_{B_{(s)}^*}}{(m_{B_{(s)}} + m_V)f_{B_{(s)}^*}} \lim_{q^2 \rightarrow m_{B_{(s)}^*}^2} \left[\left(1 - q^2/m_{B_{(s)}^*}^2\right) V(q^2) \right], \quad (63)$$

$$g_{B_{(s)}^*B_{(s)}V} = \frac{2}{f_{B_{(s)}^*}^{\perp}} \lim_{q^2 \rightarrow m_{B_{(s)}^*}^2} \left[\left(1 - q^2/m_{B_{(s)}^*}^2\right) T_1(q^2) \right]. \quad (64)$$

Employing Eq.(64) and assuming $f_{B_{(s)}^*}^T = f_{B_{(s)}^*}$, we obtain various numerical values for the coupling $g_{B_{(s)}^*B_{(s)}V}$ using the $B_{(s)} \rightarrow V$ form factors from two distinct LCSRs [28, 32]. These results are summarized in Table 13.

Our study reveals a discrepancy between our central value and the projections from the transition form factors, which can be attributed to two main factors. Firstly, different theoretical calculations of form factors yield different results, leading to inconsistent conclusions [28, 32]. In Ref.[32], our results are consistent with their theoretical predictions when considering uncertainties. This consistency is attributed to the significant magnitude of the uncertainties. However, in Ref.[28], notable

Method	This work	$V(q^2)$ [28]	$V(q^2)$ [32]	$T_1(q^2)$ [28]	$T_1(q^2)$ [32]
$g_{B^*B\rho}$	$3.00^{+0.49}_{-0.44}$	$7.24^{+1.38}_{-1.26}$	$5.51^{+3.69}_{-2.34}$	$6.83^{+1.26}_{-1.15}$	$6.17^{+4.14}_{-2.61}$
	$3.74^{+0.38}_{-0.38}$	$8.53^{+1.44}_{-1.44}$	$6.49^{+4.31}_{-2.74}$	$8.04^{+1.31}_{-1.31}$	$7.25^{+4.83}_{-3.06}$
$g_{B^*B\omega}$	$1.88^{+0.34}_{-0.30}$	$6.78^{+1.73}_{-1.65}$	$6.00^{+4.00}_{-2.55}$	$6.50^{+1.58}_{-1.5}$	$6.69^{+4.52}_{-2.83}$
	$2.38^{+0.28}_{-0.28}$	$7.98^{+1.92}_{-1.92}$	$7.06^{+4.67}_{-2.99}$	$7.65^{+1.74}_{-1.74}$	$7.88^{+5.28}_{-3.31}$
$g_{B_s^*BK^*}$	$3.12^{+0.60}_{-0.50}$	$7.34^{+1.69}_{-1.55}$	$6.22^{+3.92}_{-2.39}$	$6.96^{+1.54}_{-1.41}$	$6.95^{+4.38}_{-2.67}$
	$3.61^{+0.40}_{-0.39}$	$8.02^{+1.60}_{-1.60}$	$6.80^{+4.21}_{-2.57}$	$7.61^{+1.44}_{-1.44}$	$7.60^{+4.71}_{-2.87}$
$g_{B^*B_sK^*}$	$3.16^{+0.52}_{-0.47}$	$6.75^{+1.42}_{-1.32}$	--	$6.43^{+1.26}_{-1.16}$	--
	$3.61^{+0.41}_{-0.40}$	$7.95^{+1.52}_{-1.52}$	--	$7.57^{+1.33}_{-1.33}$	--
$g_{B_s^*B_s\phi}$	$2.70^{+0.49}_{-0.41}$	$6.88^{+1.33}_{-1.18}$	--	$6.54^{+1.24}_{-1.09}$	--
	$2.86^{+0.32}_{-0.30}$	$7.51^{+1.18}_{-1.18}$	--	$7.15^{+1.08}_{-1.08}$	--

Table 13: Coupling constant $g_{B_{(s)}^*B_{(s)}V}$ in units of GeV^{-1} extracted from the residue of the transition form factors V and T_1 in the framework of LCSR fit, compared with our obtained values.

deviations persist even after accounting for uncertainties. Moreover, there might be an underestimation of uncertainties stemming from the parameterizations of form factors to address unphysical singularities. Secondly, assuming the validity of these findings, the Borel suppression in the double dispersion relation may not effectively eliminate contributions from isolated excitations, as discussed in Ref. [39]. In sum rule calculations, it is common practice to include contributions from higher states in the perturbative estimation of a continuum, often without explicit consideration of isolated excited states. This approach is supported by the stability criterion being met adequately without requiring substantial excitation contributions. However, Ref. [39] proposes a different viewpoint, suggesting that neglecting explicit radial excitation contributions could be the root of the discrepancy. While acknowledging the Borel suppression effect, they argue that in certain cases, such as the one under consideration, the suppression might be insufficient, leading to the need for additional considerations. Incorporating explicit radial excitation contributions to the hadronic side of the LCSRs provides a plausible explanation for the failure of the LCSR prediction. The relatively weak exponential suppression due to the Borel transformation in the LCSR framework significantly amplifies the impact of radial excitations without necessitating excessively large couplings. This suppression is significantly weaker compared to standard sum rules, primarily due to the additional factor in the exponent and the larger mean value of M^2 within the allowed range. Overall, according to Ref. [39],

assuming partial cancellation between contributions of excited and ground states in the dispersion relation may lead to an increased LCSR coupling.

When extending Eq.(64) to include transition form factors from D to V , we can derive the coupling for D^*DV as well. By employing the D to ρ form factor detailed in the Ref. [56], our calculations yielded couplings $g_{D^*D\rho}$ of $8.91_{-0.55}^{+0.77} \text{ GeV}^{-1}$ using the heavy meson decay constants from LQCD, and $8.29_{-0.51}^{+0.71} \text{ GeV}^{-1}$ using the decay constants from two-point QCDSRs, which exceed the values of $3.40_{-0.43}^{+0.49} \text{ GeV}^{-1}$ and $3.53_{-0.57}^{+0.61} \text{ GeV}^{-1}$ obtained from LCSRs a lot, mirroring the trend observed in $B \rightarrow \rho$ transitions. Nevertheless, since the Ref. [56] only provides uncertainty estimates for $V(0)$ and not for the fitting parameters a_1 and a_2 , the resulting uncertainty remains relatively small.

Finally, we also compare our results with other model-dependent studies concerning chiral and heavy quark limits. The coupling parameter λ characterizes the $H^*H\rho$ interaction, and it's related to $g_{H^*H\rho}$ through the expression,

$$\lambda = \frac{\sqrt{2}}{4} \frac{g_{H^*H\rho}}{g_V}, \quad (65)$$

where the parameter $g_V = m_\rho/f_\pi$ (m_ρ is the ρ meson mass and f_π denotes the pion decay constant) is determined from the first and second KSRF relation [3, 57, 58]. Our calculations yield $\lambda = 0.21 \pm 0.03 \text{ GeV}^{-1}$ with decay constants obtained from two-point sum rule and $\lambda = 0.20 \pm 0.03 \text{ GeV}^{-1}$ from LQCD-calculated decay constants at the leading power, based on our determination of $g_{B^*B\rho}$. These values are compatible with those obtained from Ref. [8, 18, 19] but significantly smaller than those predicted by the VMD model [40], where λ is estimated to be 0.56 GeV^{-1} , and the constituent quark model [59], which suggests a value of 0.47 GeV^{-1} . One possible reason for this discrepancy could be the likelihood of larger uncertainties in the model predictions, favoring the reliability of the LCSRs method. However, uncertainties in the determination of NLO corrections to higher-twists (such as twist-3 NLO) and sub-sub-leading power contributions remain unknown factors contributing to the observed deviation. Advancements in computational techniques, including refinements in sum rule methods and modeling, may offer valuable insights into resolving these discrepancies in the future.

6 Conclusion

In this paper, we have conducted a comprehensive investigation into the improved calculation of the strong couplings $g_{D_{(s)}^*D_{(s)}V}$ and $g_{B_{(s)}^*B_{(s)}V}$, where $V = \rho, \omega, K^*$ and ϕ , within the framework of LCSR. This framework is originally developed in Refs. [8, 9, 29], which primarily focus on the calculation of $g_{D^*D\rho}$ and $g_{B^*B\rho}$.

Our study built upon the OPE method, focusing on the correlation function Eq. (8) and incorporating vector meson LCDAs with increasing twist. We analytically derived the double spectral representation of the QCD factorization formula, employing the parton-hadron duality ansatz and the double Borel transformation. This allows us to establish LCSRs for both leading and sub-leading contributions, encompassing two-particle DAs up to twist-5 and three-particle DAs up to twist-4. Exploring the newly determined double spectral densities for subleading twist contributions allows us to perform conduct analytical continuum subtractions. This facilitates the development of higher-twist sum rules on the light-cone, improving the precision and scope of our analysis. Furthermore, we derived concise analytical expressions for NLO terms within the $\overline{\text{MS}}$ scheme for heavy quark mass. This ensures the applicability of our findings to both charmed and bottom mesons. Additionally, we have updated all input parameters for the LCSRs, focusing particularly on the Borel parameter M^2 , scale μ , and effective threshold s_0 . These modifications are based on newly cited data from Ref. [9], reflecting improvements in our understanding compared to the findings presented in Ref. [8].

Examining the numerically calculated LCSRs for the strong couplings g_{H^*HV} , we observed that the dominant contribution arises from twist-2. In addition, we found that the NLO corrections closely match the LO contributions at twist-three, constituting nearly 20% of the leading twist. Notably, our analysis revealed opposite signs for the NLO corrections between charm-meson and bottom-meson couplings. Our analysis also indicated that the contributions from subleading twists to charm-meson couplings, particularly from two-particle and three-particle LCDAs, are more significant than those for bottom-meson couplings.

When comparing our optimized LCSR predictions with the previous studies [8, 17, 19, 21], we found satisfactory agreement in the values obtained for the H^*HV couplings within theoretical uncertainties. Have these couplings in hand, we extracted the effective coupling λ in the $\text{HM}\chi\text{PT}$ Lagrangian, it is compatible with those obtained in Ref. [8, 18, 19] but significantly smaller than those predicted by the VMD model [40] and the constituent quark model [59]. Furthermore, we fulfilled a detailed exploration to the $SU(3)$ flavour symmetry breaking effects by comparing the H^*HV (for V is K^* , ω and ϕ) couplings with $g_{D^*D\rho}$ and $g_{B^*B\rho}$. The analysis revealed breaking effects ranging from -25% to -1.8% when employing the decay constants of heavy mesons calculated from LQCD, and from -13% to $+9.8\%$ when utilizing the decay constants obtained from two-point QCDSRs. Where, both $g_{H^*H\omega}$ and $g_{H_s^*H_s\phi}$ demonstrate negative symmetry breaking effects, however the breaking effects of $g_{H^*H_sK^*}$ and $g_{H_s^*HK^*}$ exhibit opposite signs for the heavy meson decay constants computed from the two methods. The most obvious $SU(3)_F$ breaking effects were observed in the coupling $g_{D_s^*D_s\phi}$ which reach to -25% , this is primarily due to the involvement of the maximum number of strange quarks in this channel. Moreover, we performed a comprehensive investigation of $g_{B_{(s)}^*B_{(s)}V}$ and $g_{D^*D\rho}$ derived from $B \rightarrow V$ [28, 32] and $D \rightarrow \rho$ transition form factors by using dispersion

relation. Which demonstrated an obvious deviation from our findings in LCSRs and the results obtained in the previous studies [8, 17, 19, 21].

Developing the LCSRs for the strong coupling g_{H^*HV} beyond our current investigation offers several promising directions. Firstly, it's crucial to calculate NLO QCD corrections to the higher-twist contributions of the vector meson DAs, this is important for clarifying the discrepancies observed in g_{H^*HV} between the direct LCSRs calculations and the indirect predictions from the $H \rightarrow V$ transition form factors. Secondly, updating the non-perturbative parameters in the conformal expansion of vector meson DAs holds significant phenomenological importance and can enhance the accuracy of our LCSRs predictions. As noticed in [9], a twist-2 model for pion LCDA was proposed from the LQCD data [60], which has led to a notable improvement in predictions for $B^*B\pi$. Another potential solution to this problem is to incorporate high excited heavy-meson states in the hadronic components of the sum rules, as suggested in the case of $D^*D\pi$ [39].

7 Acknowledgments

We appreciate the useful discussions with Chao Wang and Yu-Ming Wang. This work is supported by the National Natural Science Foundation of China with Grant No. 12075125 and 12247162. H. Y. Jiang gratefully acknowledges financial support from China Scholarship Council.

A The definitions of the vector meson LCDAs

Vector meson LCDAs are defined through expansions based on matrix elements, specifically involving the DAs of quark-antiquark (or quark-antiquark-gluon) within the vector meson. These DAs are characterized by increasing twists. The widely accepted standard definition is applied for the two-particle LCDAs of vector mesons from twist-2 to twist-5:

$$\begin{aligned}
\langle V(p, \eta^*) | \bar{q}_1(x) \gamma_\mu q_2(0) | 0 \rangle &= f_V^\parallel m_V \int_0^1 du e^{iup \cdot x} \\
&\times \left\{ p_\mu \frac{\eta^* \cdot x}{p \cdot x} \left[\phi_{2;V}^\parallel(u) - \phi_{3;V}^\perp(u) + \frac{m_V^2 x^2}{16} (\phi_{4;V}^\parallel(u) - \phi_{5;V}^\perp(u)) \right] \right. \\
&\left. + \eta_\mu^* \left(\phi_{3;V}^\perp(u) + \frac{m_V^2 x^2}{16} \phi_{5;V}^\perp(u) \right) - \frac{\eta^* \cdot x}{2(p \cdot x)^2} x_\mu m_V^2 \left(\phi_{4;V}^\parallel(u) - 2\phi_{3;V}^\perp(u) + \phi_{2;V}^\parallel(u) \right) \right\}, \quad (66) \\
\langle V(p, \eta^*) | \bar{q}_1(x) \sigma_{\mu\nu} q_2(0) | 0 \rangle &= -if_V^\perp \int_0^1 du e^{iup \cdot x} \left\{ (\eta_\mu^* p_\nu - \eta_\nu^* p_\mu) \left[\phi_{2;V}^\perp(u) + \frac{m_V^2 x^2}{16} \phi_{4;V}^\perp(u) \right] \right. \\
&\left. + (p_\mu x_\nu - p_\nu x_\mu) \frac{\eta^* \cdot x}{(p \cdot x)^2} m_V^2 \left(\phi_{3;V}^\parallel(u) - \frac{1}{2} \phi_{2;V}^\perp(u) - \frac{1}{2} \phi_{4;V}^\perp(u) \right) \right\}
\end{aligned}$$

$$+ \frac{\eta_\mu^* x_\nu - \eta_\nu^* x_\mu}{2p \cdot x} m_V^2 \left(\psi_{4;V}^\perp(u) - \phi_{2;V}^\perp(u) \right) \Big\}, \quad (67)$$

$$\langle V(p, \eta^*) | \bar{q}_1(x) \gamma_\mu \gamma_5 q_2(0) | 0 \rangle = \frac{1}{4} f_V^\parallel m_V \epsilon_{\mu\nu\rho\sigma} \eta^{*\nu} p^\rho x^\sigma \int_0^1 du e^{iup \cdot x} \left(\psi_{3;V}^\perp(u) + \frac{m_V^2 x^2}{16} \psi_{5;V}^\perp(u) \right), \quad (68)$$

$$\langle V(p, \eta^*) | \bar{q}_1(x) q_2(0) | 0 \rangle = -\frac{i}{2} f_V^\perp (\eta \cdot x) m_V^2 \int_0^1 du e^{iup \cdot x} \psi_{3;V}^\parallel(u). \quad (69)$$

The definitions of f_V^\parallel and f_V^\perp are given by:

$$\langle V(p, \eta^*) | \bar{q}_1(0) \gamma_\mu q_2(0) | 0 \rangle = f_V^\parallel m_V \eta_\mu^*, \quad \langle V(p, \eta^*) | \bar{q}_1(0) \sigma_{\mu\nu} q_2(0) | 0 \rangle = -i f_V^\perp (\eta_\mu^* p_\nu - \eta_\nu^* p_\mu). \quad (70)$$

The three-particle chiral-even DAs [51] are defined by the following matrix elements

$$\begin{aligned} \langle V(p, \eta^*) | \bar{q}_1(x) g_s G_{\mu\nu}(vx) \gamma_\alpha q_2(-x) | 0 \rangle &= i f_V^\parallel m_V P_\alpha [P_\nu \eta_{\perp\mu}^* - P_\mu \eta_{\perp\nu}^*] \Phi_{3;V}^\parallel(v, Px) \\ &+ i f_V^\parallel m_V^3 \frac{\eta^* \cdot x}{P \cdot x} [P_\mu g_{\alpha\nu}^\perp - P_\nu g_{\alpha\mu}^\perp] \Phi_{4;V}^\parallel(v, Px) \\ &+ i f_V^\parallel m_V^3 \frac{\eta^* \cdot x}{(P \cdot x)^2} P_\alpha [P_\mu x_\nu - P_\nu x_\mu] \Psi_{4;V}^\parallel(v, Px), \end{aligned} \quad (71)$$

$$\begin{aligned} \langle V(p, \eta^*) | \bar{q}_1(x) g_s \tilde{G}_{\mu\nu}(vx) \gamma_\alpha \gamma_5 q_2(-x) | 0 \rangle &= -f_V^\parallel m_V P_\alpha [P_\nu \eta_{\perp\mu}^* - P_\mu \eta_{\perp\nu}^*] \tilde{\Phi}_{3;V}^\parallel(v, Px) \\ &- f_V^\parallel m_V^3 \frac{\eta^* \cdot x}{P \cdot x} [P_\mu g_{\alpha\nu}^\perp - P_\nu g_{\alpha\mu}^\perp] \tilde{\Phi}_{4;V}^\parallel(v, Px) \\ &- f_V^\parallel m_V^3 \frac{\eta^* \cdot x}{(P \cdot x)^2} P_\alpha [P_\mu x_\nu - P_\nu x_\mu] \tilde{\Psi}_{4;V}^\parallel(v, Px), \end{aligned} \quad (72)$$

and the three-particle chiral-odd DAs[51] can be defined as

$$\begin{aligned} &\langle V(p, \eta^*) | \bar{q}_1(x) g_s G_{\mu\nu}(vx) \sigma_{\alpha\beta} q_2(-x) | 0 \rangle \\ &= f_V^\perp m_V^2 \frac{\eta^* \cdot x}{2(P \cdot x)} [P_\alpha P_\mu g_{\beta\nu}^\perp - P_\beta P_\mu g_{\alpha\nu}^\perp - P_\alpha P_\nu g_{\beta\mu}^\perp + P_\beta P_\nu g_{\alpha\mu}^\perp] \Phi_{3;V}^\perp(v, Px) \\ &+ f_V^\perp m_V^2 [P_\alpha \eta_{\perp\mu}^* g_{\beta\nu}^\perp - P_\beta \eta_{\perp\mu}^* g_{\alpha\nu}^\perp - P_\alpha \eta_{\perp\nu}^* g_{\beta\mu}^\perp + P_\beta \eta_{\perp\nu}^* g_{\alpha\mu}^\perp] \Phi_{4;V}^{\perp(1)}(v, Px) \\ &+ f_V^\perp m_V^2 [P_\mu \eta_{\perp\alpha}^* g_{\beta\nu}^\perp - P_\mu \eta_{\perp\beta}^* g_{\alpha\nu}^\perp - P_\nu \eta_{\perp\alpha}^* g_{\beta\mu}^\perp + P_\nu \eta_{\perp\beta}^* g_{\alpha\mu}^\perp] \Phi_{4;V}^{\perp(2)}(v, Px) \\ &+ \frac{f_V^\perp m_V^2}{P \cdot x} [P_\alpha P_\mu \eta_{\perp\beta}^* x_\nu - P_\beta P_\mu \eta_{\perp\alpha}^* x_\nu - P_\alpha P_\nu \eta_{\perp\beta}^* x_\mu + P_\beta P_\nu \eta_{\perp\alpha}^* x_\mu] \Phi_{4;V}^{\perp(3)}(v, Px) \\ &+ \frac{f_V^\perp m_V^2}{P \cdot x} [P_\alpha P_\mu \eta_{\perp\nu}^* x_\beta - P_\beta P_\mu \eta_{\perp\nu}^* x_\alpha - P_\alpha P_\nu \eta_{\perp\mu}^* x_\beta + P_\beta P_\nu \eta_{\perp\mu}^* x_\alpha] \Phi_{4;V}^{\perp(4)}(v, Px), \end{aligned} \quad (73)$$

$$\langle V(p, \eta^*) | \bar{q}_1(x) g_s G_{\mu\nu}(vx) q_2(-x) | 0 \rangle = -i f_V^\perp m_V^2 [\eta_{\perp\mu}^* P_\nu - \eta_{\perp\nu}^* P_\mu] \Psi_{4;V}^\perp(v, Px), \quad (74)$$

$$\langle V(p, \eta^*) | \bar{q}_1(x) g_s \tilde{G}_{\mu\nu}(vx) \gamma_5 q_2(-x) | 0 \rangle = f_V^\perp m_V^2 [\eta_{\perp\mu}^* P_\nu - \eta_{\perp\nu}^* P_\mu] \tilde{\Psi}_{4;V}^\perp(v, Px), \quad (75)$$

where

$$P_\mu = p_\mu - \frac{1}{2} x_\mu \frac{m_V^2}{P \cdot x}, \quad (76)$$

$$\eta_\mu^* = \frac{\eta^* \cdot x}{P \cdot x} \left(P_\mu - \frac{m_V^2}{2P \cdot x} x_\mu \right) + \eta_{\perp\mu}^*, \quad (77)$$

$$g_{\mu\nu}^\perp = g_{\mu\nu} - \frac{1}{P \cdot x} (P_\mu x_\nu + P_\nu x_\mu), \quad (78)$$

$$\Phi_{3p}(v, Px) = \int \mathcal{D}\underline{\alpha} e^{iP \cdot x(\alpha_1 - \alpha_2 + v\alpha_3)} \Phi_{3p}(\alpha_1, \alpha_2, \alpha_3), \quad (79)$$

$\underline{\alpha}$ is the set of three momentum fractions $\underline{\alpha} = \{\alpha_1, \alpha_2, \alpha_3\}$. The integration measure is defined as

$$\int \mathcal{D}\underline{\alpha} \equiv \int_0^1 d\alpha_1 \int_0^1 d\alpha_2 \int_0^1 d\alpha_3 \delta\left(1 - \sum \alpha_i\right). \quad (80)$$

P and x are two introduced light-like vectors and the dual gluon field strength tensor is defined as $\tilde{G}_{\mu\nu} = \frac{1}{2} \epsilon_{\mu\nu\rho\sigma} G^{\rho\sigma}$, with $\epsilon_{0123} = -1$.

B Parameterizations for the vector meson DAs

The parameterizations for the vector meson DAs in the numerical analysis are collected below:

- the twist-2 DA:

$$\phi_{2;V}^{\parallel,\perp}(u, \mu) = 6u\bar{u} \left\{ 1 + \sum_{n=1}^{\infty} a_n^{\parallel,\perp}(\mu) C_n^{3/2}(u - \bar{u}) \right\}, \quad (81)$$

in terms of the (non-perturbative) Gegenbauer moments $a_n^{\parallel,\perp}$ and the Gegenbauer polynomials $C_n^{3/2}$. To leading-logarithmic accuracy, the $a_n^{\parallel,\perp}$ renormalise multiplicatively as

$$a_n^{\parallel,\perp}(\mu) = E_{n,\text{LO}}^{\parallel,\perp}(\mu, \mu_0) a_n^{\parallel,\perp}(\mu_0). \quad (82)$$

To next-to-leading order accuracy, the scale dependence of the Gegenbauer moments is more complicated and reads [47, 50]

$$\left[f_V^\perp(\mu) a_{n,\text{NLO}}^\perp(\mu) \right] = E_{n,\text{NLO}}^\perp(\mu, \mu_0) \left[f_V^\perp(\mu_0) a_n^\perp(\mu_0) \right] + \frac{\alpha_s}{4\pi} \sum_{k=0}^{n-2} E_{n,\text{LO}}^\perp(\mu, \mu_0) d_n^k(\mu, \mu_0) \left[f_V^\perp(\mu_0) a_k^\perp(\mu_0) \right],$$

$$a_{n,\text{NLO}}^{\parallel}(\mu) = E_{n,\text{NLO}}^{\parallel}(\mu, \mu_0) a_n^{\parallel}(\mu_0) + \frac{\alpha_s}{4\pi} \sum_{k=0}^{n-2} E_{n,\text{LO}}^{\parallel}(\mu, \mu_0) d_n^k(\mu, \mu_0) a_k^{\parallel}(\mu_0), \quad (83)$$

where the formulas for the RG factors $E_{n,(N)\text{LO}}^{\parallel,\perp}(\mu, \mu_0)$ and off-diagonal mixing coefficients $d_n^k(\mu, \mu_0)$ within the $\overline{\text{MS}}$ scheme are explicitly provided in references [47, 50]. The evolution of $a_n^{\perp}(\mu)$ is closely linked to $f_V^{\perp}(\mu)$ because of the definition of the conformal operator.

- the twist-3 two-particle DAs[61]:

$$\begin{aligned} \psi_{3;V}^{\perp}(u, \mu) = & 6u\bar{u} \left\{ 1 + \left(\frac{1}{3}a_1^{\parallel}(\mu) + \frac{20}{9}\kappa_{3V}^{\parallel}(\mu) \right) C_1^{3/2}(u - \bar{u}) \right. \\ & + \left(\frac{1}{6}a_2^{\parallel}(\mu) + \frac{10}{9}\zeta_{3V}^{\parallel}(\mu) + \frac{5}{12}\omega_{3V}^{\parallel}(\mu) - \frac{5}{24}\tilde{\omega}_{3V}^{\parallel}(\mu) \right) C_2^{3/2}(u - \bar{u}) \\ & \left. + \left(\frac{1}{4}\tilde{\lambda}_{3V}^{\parallel}(\mu) - \frac{1}{8}\lambda_{3V}^{\parallel}(\mu) \right) C_3^{3/2}(u - \bar{u}) \right\} \\ & + 6 \frac{m_{q_2}(\mu) + m_{q_1}(\mu)}{m_V} \frac{f_V^{\perp}(\mu)}{f_V^{\parallel}(\mu)} \left\{ u\bar{u}(2 + 3(u - \bar{u})a_1^{\perp}(\mu) + 2(11 - 10u\bar{u})a_2^{\perp}(\mu)) \right. \\ & \left. + \bar{u} \ln \bar{u}(1 + 3a_1^{\perp}(\mu) + 6a_2^{\perp}(\mu)) + u \ln u(1 - 3a_1^{\perp}(\mu) + 6a_2^{\perp}(\mu)) \right\} \\ & - 6 \frac{m_{q_2}(\mu) - m_{q_1}(\mu)}{m_V} \frac{f_V^{\perp}(\mu)}{f_V^{\parallel}(\mu)} \left\{ u\bar{u}(9a_1^{\perp}(\mu) + 10(u - \bar{u})a_2^{\perp}(\mu)) \right. \\ & \left. + \bar{u} \ln \bar{u}(1 + 3a_1^{\perp}(\mu) + 6a_2^{\perp}(\mu)) - u \ln u(1 - 3a_1^{\perp}(\mu) + 6a_2^{\perp}(\mu)) \right\}. \quad (84) \end{aligned}$$

The scale dependence of twist-3 parameters are as followed

$$\begin{aligned} \kappa_{3V}^{\perp}(\mu) &= L^{(C_A + \frac{4}{3}C_F)/\beta_0} \kappa_{3V}^{\perp}(\mu_0), \quad \kappa_{3V}^{\parallel}(\mu) = L^{(3C_A - \frac{1}{3}C_F)/\beta_0} \kappa_{3V}^{\parallel}(\mu_0), \\ \omega_{3V}^{\perp}(\mu) &= L^{(C_A + \frac{17}{6}C_F)/\beta_0} \omega_{3V}^{\perp}(\mu_0), \quad \lambda_{3V}^{\perp}(\mu) = L^{(\frac{10}{3}C_A + \frac{1}{6}C_F)/\beta_0} \lambda_{3V}^{\perp}(\mu_0), \\ \zeta_{3V}^{\parallel}(\mu) &= L^{(3C_A - \frac{1}{3}C_F)/\beta_0} \zeta_{3V}^{\parallel}(\mu_0), \quad (85) \end{aligned}$$

and

$$\begin{pmatrix} \frac{2}{3}\omega_{3V}^{\parallel}(\mu) - \tilde{\omega}_{3V}^{\parallel}(\mu) \\ \frac{2}{3}\omega_{3V}^{\parallel}(\mu) + \tilde{\omega}_{3V}^{\parallel}(\mu) \end{pmatrix} = \left((L^{\vec{\Gamma}_3^+})/\beta_0 \right)_D \begin{pmatrix} \frac{2}{3}\omega_{3V}^{\parallel}(\mu_0) - \tilde{\omega}_{3V}^{\parallel}(\mu_0) \\ \frac{2}{3}\omega_{3V}^{\parallel}(\mu_0) + \tilde{\omega}_{3V}^{\parallel}(\mu_0) \end{pmatrix}, \quad (86)$$

$$\begin{pmatrix} \frac{2}{3}\tilde{\lambda}_{3V}^{\parallel}(\mu) + \lambda_{3V}^{\parallel}(\mu) \\ \frac{2}{3}\tilde{\lambda}_{3V}^{\parallel}(\mu) - \lambda_{3V}^{\parallel}(\mu) \end{pmatrix} = \left((L^{\vec{\Gamma}_3^-})/\beta_0 \right)_D \begin{pmatrix} \frac{2}{3}\tilde{\lambda}_{3V}^{\parallel}(\mu_0) + \lambda_{3V}^{\parallel}(\mu_0) \\ \frac{2}{3}\tilde{\lambda}_{3V}^{\parallel}(\mu_0) - \lambda_{3V}^{\parallel}(\mu_0) \end{pmatrix}, \quad (87)$$

where D represent diagonal and $\vec{\Gamma}_3$ is the vector containing the diagonal elements of the diagonal matrix $(\Gamma_3)_D$, with

$$\begin{aligned}\Gamma_3^+ &= \begin{pmatrix} \frac{7}{3}C_A + \frac{8}{3}C_F & -\frac{2}{3}C_A + \frac{2}{3}C_F \\ -\frac{4}{3}C_A + \frac{5}{3}C_F & 4C_A + \frac{1}{6}C_F \end{pmatrix}, \\ \Gamma_3^- &= \begin{pmatrix} 4C_A + \frac{1}{6}C_F & -\frac{4}{3}C_A + \frac{5}{3}C_F \\ -\frac{2}{3}C_A + \frac{2}{3}C_F & \frac{7}{3}C_A + \frac{8}{3}C_F \end{pmatrix}.\end{aligned}\quad (88)$$

- the twist-4 two-particle DAs[53]:

$$\begin{aligned}\phi_{4;V}^\perp(u, \mu) &= 30u^2\bar{u}^2 \left\{ \left(\frac{4}{3}\zeta_{4V}^\perp(\mu) - \frac{8}{3}\tilde{\zeta}_{4V}^\perp(\mu) + \frac{2}{5} + \frac{4}{35}a_2^\perp(\mu) \right) \right. \\ &\quad + \left(\frac{3}{25}a_1^\perp(\mu) + \frac{1}{3}\kappa_{3V}^\perp(\mu) - \frac{1}{45}\lambda_{3V}^\perp(\mu) - \frac{1}{15}\theta_1^\perp(\mu) + \frac{7}{30}\theta_2^\perp(\mu) + \frac{1}{5}\tilde{\theta}_1^\perp(\mu) - \frac{3}{10}\tilde{\theta}_2^\perp(\mu) \right) \\ &\quad \times C_1^{5/2}(u - \bar{u}) + \left(\frac{3}{35}a_2^\perp(\mu) + \frac{1}{60}\omega_{3V}^\perp(\mu) \right) C_2^{5/2}(u - \bar{u}) - \frac{4}{1575}\lambda_{3V}^\perp(\mu)C_3^{5/2}(u - \bar{u}) \left. \right\} \\ &\quad + \left(5\kappa_{3V}^\perp(\mu) - a_1^\perp(\mu) - 20\tilde{\phi}_2^\perp(\mu) \right) \\ &\quad \times \left\{ -4u^3(2-u)\ln u + 4\bar{u}^3(2-\bar{u})\ln \bar{u} + \frac{1}{2}u\bar{u}(u-\bar{u}) [3(u-\bar{u})^2 - 11] \right\} \\ &\quad + \left(2\omega_{3V}^\perp(\mu) - \frac{36}{11}a_2^\perp(\mu) - \frac{252}{55}\langle\langle Q^{(1)} \rangle\rangle(\mu) - \frac{140}{11}\langle\langle Q^{(3)} \rangle\rangle(\mu) \right) \\ &\quad \times \left\{ u^3(6u^2 - 15u + 10)\ln u + \bar{u}^3(6\bar{u}^2 - 15\bar{u} + 10)\ln \bar{u} - \frac{1}{8}u\bar{u} [13(u-\bar{u})^2 - 21] \right\}.\end{aligned}\quad (89)$$

- the twist-4 three-particle DAs³

$$\begin{aligned}\Psi_{4;V}^\perp(\alpha_i, \mu) &= 30\alpha_3^2 \left\{ \psi_0^\perp(\mu)(1 - \alpha_3) + \psi_1^\perp(\mu) [\alpha_3(1 - \alpha_3) - 6\alpha_1\alpha_2] \right. \\ &\quad + \psi_2^\perp(\mu) \left[\alpha_3(1 - \alpha_3) - \frac{3}{2}(\alpha_1^2 + \alpha_2^2) \right] + (\alpha_1 - \alpha_2) \left[\theta_0^\perp(\mu) + \alpha_3\theta_1^\perp(\mu) + \frac{1}{2}(5\alpha_3 - 3)\theta_2^\perp(\mu) \right] \left. \right\}, \\ \tilde{\Psi}_{4;V}^\perp(\alpha_i, \mu) &= 30\alpha_3^2 \left\{ \tilde{\psi}_0^\perp(\mu)(1 - \alpha_3) + \tilde{\psi}_1^\perp(\mu) [\alpha_3(1 - \alpha_3) - 6\alpha_1\alpha_2] \right.\end{aligned}$$

³We adopt a convention denoted as $\underline{\alpha} = \{\alpha_1, \alpha_2, \alpha_3\} = \{\alpha_{\bar{q}_1}, \alpha_{q_2}, \alpha_g\}$. It's worth mentioning that this differs from the convention used in Ref.[53] where the only distinction is the exchange of α_1 for α_2 .

$$\begin{aligned}
& + \tilde{\psi}_2^\perp(\mu) \left[\alpha_3(1 - \alpha_3) - \frac{3}{2}(\alpha_1^2 + \alpha_2^2) \right] + (\alpha_1 - \alpha_2) \left[\tilde{\theta}_0^\perp(\mu) + \alpha_3 \tilde{\theta}_1^\perp(\mu) + \frac{1}{2}(5\alpha_3 - 3)\tilde{\theta}_2^\perp(\mu) \right] \Big\}, \\
\Phi_{4;V}^{\perp(1)}(\alpha_i, \mu) &= 120\alpha_1\alpha_2\alpha_3[\phi_0^\perp(\mu) - \phi_1^\perp(\mu)(\alpha_1 - \alpha_2) + \phi_2^\perp(\mu)(3\alpha_3 - 1)], \\
\Phi_{4;V}^{\perp(2)}(\alpha_i, \mu) &= -30\alpha_3^2 \left\{ \tilde{\theta}_0^\perp(\mu)(1 - \alpha_3) + \tilde{\theta}_1^\perp(\mu) [\alpha_3(1 - \alpha_3) - 6\alpha_1\alpha_2] \right. \\
& \quad \left. + \tilde{\theta}_2^\perp(\mu) \left[\alpha_3(1 - \alpha_3) - \frac{3}{2}(\alpha_1^2 + \alpha_2^2) \right] + (\alpha_1 - \alpha_2) \left[\tilde{\psi}_0^\perp(\mu) + \alpha_3 \tilde{\psi}_1^\perp(\mu) + \frac{1}{2}(5\alpha_3 - 3)\tilde{\psi}_2^\perp(\mu) \right] \right\}, \\
\Phi_{4;V}^{\perp(3)}(\alpha_i, \mu) &= -120\alpha_1\alpha_2\alpha_3[\tilde{\phi}_0^\perp(\mu) - \tilde{\phi}_1^\perp(\mu)(\alpha_1 - \alpha_2) + \tilde{\phi}_2^\perp(\mu)(3\alpha_3 - 1)], \\
\Phi_{4;V}^{\perp(4)}(\alpha_i, \mu) &= 30\alpha_3^2 \left\{ \theta_0^\perp(\mu)(1 - \alpha_3) + \theta_1^\perp(\mu) [\alpha_3(1 - \alpha_3) - 6\alpha_1\alpha_2] \right. \\
& \quad \left. + \theta_2^\perp(\mu) \left[\alpha_3(1 - \alpha_3) - \frac{3}{2}(\alpha_1^2 + \alpha_2^2) \right] + (\alpha_1 - \alpha_2) \left[\psi_0^\perp(\mu) + \alpha_3 \psi_1^\perp(\mu) + \frac{1}{2}(5\alpha_3 - 3)\psi_2^\perp(\mu) \right] \right\}.
\end{aligned} \tag{90}$$

The parameters associated with the three particle amplitudes are as followed

$$\begin{aligned}
\psi_0^\perp(\mu) &= \zeta_{4V}^\perp(\mu), & \tilde{\psi}_0^\perp(\mu) &= \tilde{\zeta}_{4V}^\perp(\mu), \\
\phi_0^\perp(\mu) &= \frac{1}{6}\kappa_{3V}^\perp(\mu) + \frac{1}{3}\kappa_{4V}^\perp(\mu), & \tilde{\phi}_0^\perp(\mu) &= \frac{1}{6}\kappa_{3V}^\perp(\mu) - \frac{1}{3}\kappa_{4V}^\perp(\mu), \\
\theta_0^\perp(\mu) &= -\frac{1}{6}\kappa_{3V}^\perp(\mu) - \frac{1}{3}\kappa_{4V}^\perp(\mu), & \tilde{\theta}_0^\perp(\mu) &= -\frac{1}{6}\kappa_{3V}^\perp(\mu) + \frac{1}{3}\kappa_{4V}^\perp(\mu). \\
\phi_1^\perp(\mu) &= \frac{9}{44}a_2^\perp(\mu) + \frac{1}{8}\omega_{3V}^\perp(\mu) + \frac{63}{220}\langle\langle Q^{(1)} \rangle\rangle(\mu) - \frac{119}{44}\langle\langle Q^{(3)} \rangle\rangle(\mu), \\
\tilde{\phi}_1^\perp(\mu) &= -\frac{9}{44}a_2^\perp(\mu) + \frac{1}{8}\omega_{3V}^\perp(\mu) - \frac{63}{220}\langle\langle Q^{(1)} \rangle\rangle(\mu) - \frac{35}{44}\langle\langle Q^{(3)} \rangle\rangle(\mu), \\
\psi_1^\perp(\mu) &= \frac{3}{44}a_2^\perp(\mu) + \frac{1}{12}\omega_{3V}^\perp(\mu) + \frac{49}{110}\langle\langle Q^{(1)} \rangle\rangle(\mu) - \frac{7}{22}\langle\langle Q^{(3)} \rangle\rangle(\mu) + \frac{7}{3}\langle\langle Q^{(5)} \rangle\rangle(\mu), \\
\tilde{\psi}_1^\perp(\mu) &= -\frac{3}{44}a_2^\perp(\mu) + \frac{1}{12}\omega_{3V}^\perp(\mu) - \frac{49}{110}\langle\langle Q^{(1)} \rangle\rangle(\mu) + \frac{7}{22}\langle\langle Q^{(3)} \rangle\rangle(\mu) + \frac{7}{3}\langle\langle Q^{(5)} \rangle\rangle(\mu), \\
\psi_2^\perp(\mu) &= -\frac{3}{22}a_2^\perp(\mu) - \frac{1}{12}\omega_{3V}^\perp(\mu) + \frac{28}{55}\langle\langle Q^{(1)} \rangle\rangle(\mu) + \frac{7}{11}\langle\langle Q^{(3)} \rangle\rangle(\mu) + \frac{14}{3}\langle\langle Q^{(5)} \rangle\rangle(\mu), \\
\tilde{\psi}_2^\perp(\mu) &= \frac{3}{22}a_2^\perp(\mu) - \frac{1}{12}\omega_{3V}^\perp(\mu) - \frac{28}{55}\langle\langle Q^{(1)} \rangle\rangle(\mu) - \frac{7}{11}\langle\langle Q^{(3)} \rangle\rangle(\mu) + \frac{14}{3}\langle\langle Q^{(5)} \rangle\rangle(\mu). \tag{91}
\end{aligned}$$

and

$$\left(\zeta_{4V}^\perp + \tilde{\zeta}_{4V}^\perp \right) (\mu) = L^{\gamma_+/\beta_0} \left(\zeta_{4V}^\perp + \tilde{\zeta}_{4V}^\perp \right) (\mu_0), \quad \gamma_+ = 3C_A - \frac{8}{3}C_F,$$

$$\left(\zeta_{4V}^\perp - \tilde{\zeta}_{4V}^\perp\right)(\mu) = L^{\gamma_-/\beta_0} \left(\zeta_{4V}^\perp - \tilde{\zeta}_{4V}^\perp\right)(\mu_0), \quad \gamma_- = 4C_A - 4C_F. \quad (92)$$

The $\kappa_{4V}^\perp(\mu)$ depends on quark masses and $a_1^\perp(\mu)$ and was obtained in Ref. [62]. Like with $\kappa_{4V}^\parallel(\mu)$, the scale-dependence of κ_{4V}^\perp follows from that of the parameters on the right-hand side and is given by

$$\begin{aligned} \kappa_{4V}^\perp(\mu) = & \kappa_{4V}^\perp(\mu_0) + \left(L^{8/(3\beta_0)} - 1\right) \frac{1}{10} a_1^\perp(\mu_0^2) + \left(L^{8/(3\beta_0)} - 1\right) \frac{f_V^\parallel}{f_V^\perp(\mu_0)} \frac{[m_{q_2} - m_{q_1}](\mu_0^2)}{12m_V} \\ & - \left(L^{8/\beta_0} - 1\right) \frac{[m_{q_2}^2 - m_{q_1}^2](\mu_0)}{4m_V^2}, \end{aligned} \quad (93)$$

with $L = \alpha_s(\mu^2)/\alpha_s(\mu_0^2)$.

The precise definition of $\langle\langle Q^{(i)} \rangle\rangle$ is given in Ref.[51]. $\omega_{3K^*}^\perp$ is a twist-3 parameter. Existing numerical determinations of these parameters from QCD sum rules are far from being precise, so we decide to estimate them using the renormalon model of Ref.[63] instead.

The renormalon model implies the following estimates for the G-conserving twist-4 parameters:

$$\langle\langle Q^{(1)} \rangle\rangle^R = -\frac{10}{3}\zeta_{4K^*}^\perp, \quad \langle\langle Q^{(3)} \rangle\rangle^R = -\zeta_{4K^*}^\perp, \quad \langle\langle Q^{(5)} \rangle\rangle^R = 0. \quad (94)$$

- the twist-5 two-particle DAs(asymptotic form)[28]:

$$\psi_{5;V}^\perp(u) = 12u^2\bar{u}^2. \quad (95)$$

Recall that $\bar{u} = 1 - u$. The expression discussed is applicable to a $V = (q_2\bar{q}_1)$ meson. In the case of $\bar{V} = (q_1\bar{q}_2)$, one must replace u with $1 - u$ and exchange the values of m_{q_2} and m_{q_1} .

C Double spectral density and integral at NLO

The expression for the twist-2 component of the Next-to-Leading Order (NLO) double spectral density in the sum rule (47) is obtained from the calculations presented in Ref.[29]. The analytical expression for the double spectral density can be collected:

$$\begin{aligned} \rho^{\text{NLO}}(s_1, s_2) = & \frac{1}{m_Q} \left\{ [\rho_{\text{I}}(r, \sigma) + \rho_{\text{II}}(r, \sigma) \ln r + \rho_{\text{III}}(r, \sigma) (\ln^2 r - \pi^2)] \delta^{(2)}(r - 1) \right. \\ & \left. + [\rho_{\text{II}}(r, \sigma) + 2\rho_{\text{III}}(r, \sigma) \ln r] \frac{d^3}{dr^3} \ln |1 - r| \right\} \theta(s_1 - m_Q^2) \theta(s_2 - m_Q^2), \end{aligned} \quad (96)$$

where the invariant functions have been introduced,

$$\rho_{\text{I}}(r, \sigma) = \frac{(r+1)}{\sigma^3} \left\{ 6r\sigma^2 \left[2 \ln \left(\frac{\mu^2}{m_Q^2} \right) + \frac{3}{2} \ln \left(\frac{\nu^2}{\mu^2} \right) + 3 \text{Li}_2 \left(-\frac{\sigma}{r+1} \right) + \text{Li}_2 \left(-\frac{r\sigma}{r+1} \right) \right] \right.$$

$$\begin{aligned}
& + 6r\sigma^2 \ln\left(\frac{\sigma}{r+1}\right) \left[\ln\left(\frac{\sigma+r+1}{r+1}\right) + \ln\left(\frac{r\sigma+r+1}{r+1}\right) \right] \\
& + 3(r+1) [2r(\sigma+1) + 5\sigma + 2] \ln\left(\frac{\sigma+r+1}{r+1}\right) \\
& - \frac{3r\sigma^2}{(r+\sigma+1)(r\sigma+r+1)} [9r\sigma^2 + (7r+10)(r+1)\sigma + 8(r+1)^2] \ln\left(\frac{\sigma}{r+1}\right) \\
& + \frac{\sigma}{r+\sigma+1} \left[((3+2\pi^2)r+6)\sigma^2 + ((9+2\pi^2)r-6)(r+1)\sigma - 6(r+1)^2 \right] \Bigg\}, \\
\rho_{\text{II}}(r, \sigma) &= 3r(r+1) \left[\frac{r}{r\sigma+r+1} + \frac{2}{r+\sigma+1} - \frac{2}{\sigma} \ln\left(\frac{\sigma+r+1}{r\sigma+r+1}\right) \right], \\
\rho_{\text{III}}(r, \sigma) &= -\frac{6r(r+1)}{\sigma}, \tag{97}
\end{aligned}$$

with the introduction of two new dimensionless variables carried out through the following definitions:

$$r = \frac{s_1 - m_Q^2}{s_2 - m_Q^2}, \quad \sigma = \frac{s_1}{m_Q^2} + \frac{s_2}{m_Q^2} - 2. \tag{98}$$

Switching to the pole-mass scheme of the heavy quark, one needs to add the following expression

$$\Delta\rho_{\text{pole}}^{(\text{tw}2, \text{NLO})}(r, \sigma) = 6m_Q^4 \left[4 + 3 \ln\left(\frac{\mu^2}{m_Q^2}\right) \right] \frac{d}{dm_Q^2} \left[\frac{1}{m_Q^2} \frac{r(r+1)}{\sigma} \right]. \tag{99}$$

Finally, for completeness we present the pole-mass scheme additions to the final NLO expressions in (56):

$$\Delta f_{\text{pole}}^{(\text{tw}2)}(\sigma) = 3 \left(4 + 3 \ln\frac{\mu^2}{m_Q^2} \right) \exp\left(-\frac{m_Q^2}{M^2}\right). \tag{100}$$

References

- [1] Mark B. Wise. Chiral perturbation theory for hadrons containing a heavy quark. *Phys. Rev. D*, 45(7):R2188, 1992.
- [2] Gustavo Burdman and John F. Donoghue. Union of chiral and heavy quark symmetries. *Phys. Lett. B*, 280:287–291, 1992.
- [3] R. Casalbuoni, A. Deandrea, N. Di Bartolomeo, Raoul Gatto, F. Feruglio, and G. Nardulli. Phenomenology of heavy meson chiral Lagrangians. *Phys. Rept.*, 281:145–238, 1997.

- [4] Tung-Mow Yan, Hai-Yang Cheng, Chi-Yee Cheung, Guey-Lin Lin, Y. C. Lin, and Hoi-Lai Yu. Heavy quark symmetry and chiral dynamics. *Phys. Rev. D*, 46:1148–1164, 1992. [Erratum: *Phys.Rev.D* 55, 5851 (1997)].
- [5] Hai-Yang Cheng, Chun-Khiang Chua, and Amarjit Soni. Final state interactions in hadronic B decays. *Phys. Rev. D*, 71:014030, 2005.
- [6] I. Sentitemsu Imsong, Alexander Khodjamirian, Thomas Mannel, and Danny van Dyk. Extrapolation and unitarity bounds for the $B \rightarrow \pi$ form factor. *JHEP*, 02:126, 2015.
- [7] Xin-Qiang Li, Fang Su, and Ya-Dong Yang. Determination of the strong coupling $g_{B^*B\pi}$ from semi-leptonic $B \rightarrow \pi\ell\nu$ decay. *Phys. Rev. D*, 83:054019, 2011.
- [8] Chao Wang and Hua-Dong Li. $D^*D\rho$ and $B^*B\rho$ strong couplings in light-cone sum rules. *Chin. Phys. C*, 44(7):073103, 2020.
- [9] Alexander Khodjamirian, Blaženka Melić, Yu-Ming Wang, and Yan-Bing Wei. The $D^*D\pi$ and $B^*B\pi$ couplings from light-cone sum rules. *JHEP*, 03:016, 2021.
- [10] Mikhail A. Shifman, A. I. Vainshtein, and Valentin I. Zakharov. QCD and Resonance Physics. Theoretical Foundations. *Nucl. Phys. B*, 147:385–447, 1979.
- [11] Mikhail A. Shifman, A. I. Vainshtein, and Valentin I. Zakharov. QCD and Resonance Physics: Applications. *Nucl. Phys. B*, 147:448–518, 1979.
- [12] Pietro Colangelo and Alexander Khodjamirian. QCD sum rules, a modern perspective. *arXiv*, hep-ph/0010175:1495–1576, 10 2000.
- [13] I. I. Balitsky, Vladimir M. Braun, and A. V. Kolesnichenko. Radiative Decay $\Sigma^+ \rightarrow p\gamma$ in Quantum Chromodynamics. *Nucl. Phys. B*, 312:509–550, 1989.
- [14] Vladimir M. Braun and I. E. Filyanov. QCD Sum Rules in Exclusive Kinematics and Pion Wave Function. *Z. Phys. C*, 44:157, 1989.
- [15] V. L. Chernyak and I. R. Zhitnitsky. B meson exclusive decays into baryons. *Nucl. Phys. B*, 345:137–172, 1990.
- [16] T. M. Aliev, Durmus A. Demir, E. Iltan, and N. K. Pak. $g_{B^*B\rho}$ and $g_{D^*D\rho}$ coupling constants in light cone QCD sum rules. *Phys. Rev. D*, 53:355–360, 1996.
- [17] Zuo-Hong Li, Tao Huang, Jin-Zuo Sun, and Zhen-Hong Dai. Strong couplings of heavy mesons to a light vector meson in QCD. *Phys. Rev. D*, 65:076005, 2002.

- [18] Zuo-Hong Li, Wei Liu, and Hai-Yan Liu. Systematic Study on QCD Interactions of Heavy Mesons with rho Meson. *Phys. Lett. B*, 659:598–606, 2008.
- [19] Zhi-Gang Wang. Analysis of the vertices DDV and D^*DV with light-cone QCD sum rules. *Eur. Phys. J. C*, 52:553–560, 2007.
- [20] Zhi-Gang Wang. Analysis of the vertices $D^*D^*\pi$ and $D^*D_s^*K$ with light-cone QCD sum rules. *Nucl. Phys. A*, 796:61–82, 2007.
- [21] K. Azizi and H. Sundu. $g_{D_s^*DK^*(892)}$ and $g_{B_s^*BK^*(892)}$ coupling constants in QCD sum rules. *J. Phys. G*, 38:045005, 2011.
- [22] B. Osorio Rodrigues, M. E. Bracco, M. Nielsen, and F. S. Navarra. $D^*D\rho$ vertex from QCD sum rules. *Nucl. Phys. A*, 852:127–140, 2011.
- [23] R. Khosravi and M. Janbazi. Analysis of $VD_{s_0}^*D_{s_1}$ and $VD_sD_s^*$ vertices. *Phys. Rev. D*, 89(1):016001, 2014.
- [24] Alexander Khodjamirian, Blaženka Melić, and Yu-Ming Wang. A guide to the QCD light-cone sum rule for b -quark decays. *arXiv*, 2311.08700, 11 2023.
- [25] Patricia Ball and Roman Zwicky. New results on $B \rightarrow \pi, K, \eta$ decay formfactors from light-cone sum rules. *Phys. Rev. D*, 71:014015, 2005.
- [26] G. Duplancic, A. Khodjamirian, Th. Mannel, B. Melic, and N. Offen. Light-cone sum rules for $B \rightarrow \pi$ form factors revisited. *JHEP*, 04:014, 2008.
- [27] Patricia Ball and Roman Zwicky. $B_{d,s} \rightarrow \rho, \omega, K^*, \phi$ decay form-factors from light-cone sum rules revisited. *Phys. Rev. D*, 71:014029, 2005.
- [28] Aoife Bharucha, David M. Straub, and Roman Zwicky. $B \rightarrow V\ell^+\ell^-$ in the Standard Model from light-cone sum rules. *JHEP*, 08:098, 2016.
- [29] Hua-Dong Li, Cai-Dian Lü, Chao Wang, Yu-Ming Wang, and Yan-Bing Wei. QCD calculations of radiative heavy meson decays with subleading power corrections. *JHEP*, 04:023, 2020.
- [30] Yu-Ming Wang and Yue-Long Shen. QCD corrections to $B \rightarrow \pi$ form factors from light-cone sum rules. *Nucl. Phys. B*, 898:563–604, 2015.
- [31] Bo-Yan Cui, Yong-Kang Huang, Yue-Long Shen, Chao Wang, and Yu-Ming Wang. Precision calculations of $B_{d,s} \rightarrow \pi, K$ decay form factors in soft-collinear effective theory. *JHEP*, 03:140, 2023.

- [32] Jing Gao, Cai-Dian Lü, Yue-Long Shen, Yu-Ming Wang, and Yan-Bing Wei. Precision calculations of $B \rightarrow V$ form factors from soft-collinear effective theory sum rules on the light-cone. *Phys. Rev. D*, 101(7):074035, 2020.
- [33] Thorsten Feldmann and Matthew W. Y. Yip. Form factors for $\Lambda_b \rightarrow \Lambda$ transitions in the soft-collinear effective theory. *Phys. Rev. D*, 85:014035, 2012. [Erratum: Phys.Rev.D 86, 079901 (2012)].
- [34] Yu-Ming Wang and Yue-Long Shen. Perturbative Corrections to $\Lambda_b \rightarrow \Lambda$ Form Factors from QCD Light-Cone Sum Rules. *JHEP*, 02:179, 2016.
- [35] Jing Gao, Tobias Huber, Yao Ji, Chao Wang, Yu-Ming Wang, and Yan-Bing Wei. $B \rightarrow D\ell\nu_\ell$ form factors beyond leading power and extraction of $|V_{cb}|$ and $R(D)$. *JHEP*, 05:024, 2022.
- [36] Bo-Yan Cui, Yong-Kang Huang, Yu-Ming Wang, and Xue-Chen Zhao. Shedding new light on $R(D_{(s)}^{(*)})$ and $|V_{cb}|$ from semileptonic $B_{(s)} \rightarrow D_{(s)}^{(*)}\ell\nu_\ell$ decays. *Phys. Rev. D*, 108(7):L071504, 2023.
- [37] Yu-Ming Wang and Yue-Long Shen. Subleading-power corrections to the radiative leptonic $B \rightarrow \gamma\ell\nu$ decay in QCD. *JHEP*, 05:184, 2018.
- [38] Bo-Yan Cui, Yue-Long Shen, Chao Wang, and Yan-Bing Wei. QCD factorization for the $B \rightarrow \gamma\ell\nu_\ell$ decay beyond leading power. *arXiv*, 2308.16436, 2023.
- [39] D. Becirevic, J. Charles, A. LeYaouanc, L. Oliver, O. Pene, and J. C. Raynal. Possible explanation of the discrepancy of the light cone QCD sum rule calculation of $g_{(D^*D\pi)}$ coupling with experiment. *JHEP*, 01:009, 2003.
- [40] Claudia Isola, Massimo Ladisa, Giuseppe Nardulli, and Pietro Santorelli. Charming penguins in $B \rightarrow K^*\pi, K(\rho, \omega, \phi)$ decays. *Phys. Rev. D*, 68:114001, 2003.
- [41] K. G. Chetyrkin, Johann H. Kuhn, and M. Steinhauser. RunDec: A Mathematica package for running and decoupling of the strong coupling and quark masses. *Comput. Phys. Commun.*, 133:43–65, 2000.
- [42] Patrick Gelhausen, Alexander Khodjamirian, Alexei A. Pivovarov, and Denis Rosenthal. Decay constants of heavy-light vector mesons from QCD sum rules. *Phys. Rev. D*, 88:014015, 2013. [Erratum: Phys.Rev.D 89, 099901 (2014), Erratum: Phys.Rev.D 91, 099901 (2015)].
- [43] V. Lubicz, A. Melis, and S. Simula. Masses and decay constants of $D_{(s)}^*$ and $B_{(s)}^*$ mesons with $N_f = 2 + 1 + 1$ twisted mass fermions. *Phys. Rev. D*, 96(3):034524, 2017.

- [44] B. Colquhoun, C. T. H. Davies, R. J. Dowdall, J. Kettle, J. Koponen, G. P. Lepage, and A. T. Lytle. B-meson decay constants: a more complete picture from full lattice QCD. *Phys. Rev. D*, 91(11):114509, 2015.
- [45] V. M. Belyaev, Vladimir M. Braun, A. Khodjamirian, and R. Ruckl. $D^*D\pi$ and $B^*B\pi$ couplings in QCD. *Phys. Rev. D*, 51:6177–6195, 1995.
- [46] M. Beneke and Vladimir A. Smirnov. Asymptotic expansion of Feynman integrals near threshold. *Nucl. Phys. B*, 522:321–344, 1998.
- [47] Yu-Ming Wang and Yue-Long Shen. Subleading power corrections to the pion-photon transition form factor in QCD. *JHEP*, 12:037, 2017.
- [48] R. L. Workman et al. Review of Particle Physics. *PTEP*, 2022:083C01, 2022.
- [49] Y. Aoki et al. FLAG Review 2021. *Eur. Phys. J. C*, 82(10):869, 2022.
- [50] S. S. Agaev, V. M. Braun, N. Offen, and F. A. Porkert. Light Cone Sum Rules for the $\pi^0\gamma^*\gamma$ Form Factor Revisited. *Phys. Rev. D*, 83:054020, 2011.
- [51] Patricia Ball and Vladimir M. Braun. Higher twist distribution amplitudes of vector mesons in QCD: Twist - 4 distributions and meson mass corrections. *Nucl. Phys. B*, 543:201–238, 1999.
- [52] Patricia Ball, Vladimir M. Braun, Y. Koike, and K. Tanaka. Higher twist distribution amplitudes of vector mesons in QCD: Formalism and twist - three distributions. *Nucl. Phys. B*, 529:323–382, 1998.
- [53] Patricia Ball, V. M. Braun, and A. Lenz. Twist-4 distribution amplitudes of the K^* and ϕ mesons in QCD. *JHEP*, 08:090, 2007.
- [54] A. Khodjamirian, Ch. Klein, Th. Mannel, and N. Offen. Semileptonic charm decays $D \rightarrow \pi l \nu_{(l)}$ and $D \rightarrow K l \nu_{(l)}$ from QCD Light-Cone Sum Rules. *Phys. Rev. D*, 80:114005, 2009.
- [55] A. Khodjamirian, Th. Mannel, N. Offen, and Y. M. Wang. $B \rightarrow \pi l \nu_l$ Width and $|V_{ub}|$ from QCD Light-Cone Sum Rules. *Phys. Rev. D*, 83:094031, 2011.
- [56] Hai-Bing Fu, Long Zeng, Rong Lü, Wei Cheng, and Xing-Gang Wu. The $D \rightarrow \rho$ semileptonic and radiative decays within the light-cone sum rules. *Eur. Phys. J. C*, 80(3):194, 2020.
- [57] Ken Kawarabayashi and Mahiko Suzuki. Partially conserved axial vector current and the decays of vector mesons. *Phys. Rev. Lett.*, 16:255, 1966.

- [58] Riazuddin and Fayyazuddin. Algebra of current components and decay widths of rho and K^* mesons. *Phys. Rev.*, 147:1071–1073, 1966.
- [59] D. Melikhov and B. Stech. Weak form-factors for heavy meson decays: An Update. *Phys. Rev. D*, 62:014006, 2000.
- [60] Gunnar S. Bali, Vladimir M. Braun, Simon Bürger, Meinulf Göckeler, Michael Gruber, Fabian Hutzler, Piotr Korcyl, Andreas Schäfer, André Sternbeck, and Philipp Wein. Light-cone distribution amplitudes of pseudoscalar mesons from lattice QCD. *JHEP*, 08:065, 2019. [Addendum: *JHEP* 11, 037 (2020)].
- [61] Patricia Ball and G. W. Jones. Twist-3 distribution amplitudes of K^* and ϕ mesons. *JHEP*, 03:069, 2007.
- [62] Patricia Ball and Roman Zwicky. Operator relations for $SU(3)$ breaking contributions to K and K^* distribution amplitudes. *JHEP*, 02:034, 2006.
- [63] Vladimir M. Braun, Einar Gardi, and Stefan Gottwald. Renormalon approach to higher twist distribution amplitudes and the convergence of the conformal expansion. *Nucl. Phys. B*, 685:171–226, 2004.